Heliyon 10 (2024) e24703

Contents lists available at ScienceDirect

Heliyon

journal homepage: www.cell.com/heliyon

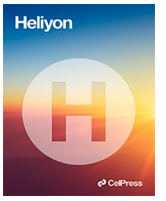

Research article

Heterozygous *Nexmif* female mice demonstrate mosaic NEXMIF expression, autism-like behaviors, and abnormalities in dendritic arborization and synaptogenesis

Margaret O'Connor [a], Hui Qiao [a], KathrynAnn Odamah [a], Pedro Casariego Cerdeira [a], Heng-Ye Man [a,b,c,*]

[a] *Department of Biology, Boston University, 5 Cummington Mall, Boston, MA 02215, USA*
[b] *Department of Pharmacology, Physiology & Biophysics, Boston University School of Medicine, 72 East Concord St., Boston, MA 02118, USA*
[c] *Center for Systems Neuroscience, Boston University, 610 Commonwealth Ave, Boston, MA 02215, USA*

A B S T R A C T

Autism spectrum disorder (ASD) is a neurodevelopmental disorder with a strong genetic basis. ASDs are commonly characterized by impairments in language, restrictive and repetitive behaviors, and deficits in social interactions. Although ASD is a highly heterogeneous disease with many different genes implicated in its etiology, many ASD-associated genes converge on common cellular defects, such as aberrant neuronal morphology and synapse dysregulation. Our previous work revealed that, in mice, complete loss of the ASD-associated X-linked gene *NEXMIF* results in a reduction in dendritic complexity, a decrease in spine and synapse density, altered synaptic transmission, and ASD-like behaviors. Interestingly, human females of *NEXMIF* haploinsufficiency have recently been reported to demonstrate autistic features; however, the cellular and molecular basis for this haploinsufficiency-caused ASD remains unclear. Here we report that in the brains of *Nexmif* $^{\pm}$ female mice, NEXMIF shows a mosaic pattern in its expression in neurons. Heterozygous female mice demonstrate behavioral impairments similar to those of knockout male mice. In the mosaic mixture of neurons from *Nexmif* $^{\pm}$ mice, cells that lack NEXMIF have impairments in dendritic arborization and spine development. Remarkably, the NEXMIF-expressing neurons from *Nexmif* $^{\pm}$ mice also demonstrate similar defects in dendritic growth and spine formation. These findings establish a novel mouse model of *NEXMIF* haploinsufficiency and provide new insights into the pathogenesis of *NEXMIF*-dependent ASD.

SIGNIFICANCE STATEMENT.

Mutations in the X-linked gene *NEXMIF* have been implicated in male individuals with autism spectrum disorders (ASD) and other neurodevelopmental defects. Recently, ASD cases of *NEXMIF* haploinsufficiency have been reported in females. To examine the neuropathobiology of *NEXMIF* haploinsufficiency, we generated heterozygous female *Nexmif* $^{\pm}$ mice which exhibit autism-like behaviors, including impaired social interaction, increased repetitive grooming, and cognitive deficits, but show no perturbations in communication behavior. In the brain, there is a mosaic pattern of NEXMIF expression without significant skewing. Remarkably, both NEXMIF+ and NEXMIF- neurons show comparable abnormalities including reductions in dendritic arborization, synapse density, and altered expression of synaptic molecules. The *Nexmif* $^{\pm}$ mouse demonstrates ASD-like behaviors and will be a valuable tool for ASD research.

1. Introduction

Autism spectrum disorders (ASD) are a class of complex neurodevelopmental disorders characterized by three hallmark features:

* Corresponding author. Department of Biology, Boston University, 5 Cummington Mall, Boston, MA 02215, USA.
E-mail address: hman@bu.edu (H.-Y. Man).

https://doi.org/10.1016/j.heliyon.2024.e24703
Received 13 March 2023; Received in revised form 28 November 2023; Accepted 12 January 2024
Available online 24 January 2024

impaired social interactions, reduced communication, and the tendency for repetitive and restrictive behaviors [1]. 25 % of ASD diagnoses have been associated with an identifiable or genetic variant, which has provided a valuable understanding of the mechanisms underlying proper neurodevelopment [2,3]. Of the hundreds of ASD-related genes in the Simmons Foundation Autism Research Initiative (SFARI) database, a considerable percentage of rare genetic variants within protein-coding genes were found to be causative in the development of ASD [4,5]. Despite this knowledge, none of the known variants can account for greater than 1 % of the total number of ASD cases, which demonstrates the complexity of ASD genetics [6–9].

NEXMIF was first studied as a candidate gene in two male members of a family who presented with autistic features and intellectual disabilities (ID) [10]. Since this original diagnosis, more cases have been reported, confirming that a loss of NEXMIF protein due to *NEXMIF* gene mutation or deletion leads to ASD [11–17]. The reported individuals with *NEXMIF*-dependent ASD show impaired communication, repetitive behaviors, seizures, ID, and microcephaly. Interestingly, although only male cases were reported in earlier studies, recent clinical reports indicate that autistic characteristics are also observed in females with *NEXMIF* mutations [17–23]. Due to infertility of affected males, females with inherited *NEXMIF* mutations are heterozygous and therefore haploinsufficient in NEXMIF. The pathogenicity of single copy *NEXMIF* gene mutation indicates that brain development and function are sensitive to the proper gene dosage of *NEXMIF*. At the cellular level, the biological function of *NEXMIF* is still under investigation. We have previously shown that loss of *Nexmif* leads to defects in neuron migration, dendritic outgrowth, and synapse formation and function [24–26]. Initial studies of *Nexmif* implicated the gene as a regulator of neural circuit formation during developmental stages and as a cytoskeletal regulator involved in neurite extension [27]. A more recent study found that loss of *Nexmif* led to a reduced number of proliferating beta cells in the mouse pancreas via downregulation of *H3f3b*, a gene whose protein (histone H3.3) has been shown to suppress retrotransposition-induced genetic variation [28,29]. Given these findings, *NEXMIF* may play a role in regulating the transcription of genes involved in neuron morphology and maintenance of genomic stability.

Notably, as an X-linked gene, *NEXMIF* presents a particular genetic situation contributing to protein haploinsufficiency. In females, one of the two X chromosomes is inactivated (XCI) to balance gene dosage between sexes. XCI is typically random, and as a result, heterozygous female individuals become mosaics of cells expressing either the normal or mutant allele. This creates two populations of neurons in the brains of heterozygous females: those that express NEXMIF (NEXMIF^{+}) and those that have inactivated the X chromosome carrying the normal allele and thus do not express NEXMIF (NEXMIF^{-}). Under this condition, despite expression of the gene product in a portion of neurons in the brain, the overall neural network can be compromised by the aberrant assembling of NEXMIF^{+} and NEXMIF^{-} neurons. Due to the randomness of XCI, the extent of NEXMIF expression can vary in the affected individuals and at the level of specific organs or tissues, resulting in a broad range of disease severity. In some X-linked gene disorders, one parental-specific X chromosome is preferentially inactivated, leading to skewed XCI activity. It has been reported that the majority of females with *NEXMIF* ASD variants had random XCI, suggesting a lack of compensatory regulation in XCI in *NEXMIF* haploinsufficient females [13,16–18,20,21,30].

Here we characterize the behavioral and cognitive abnormalities of, and investigate the related cellular defects in, the NEXMIF heterozygous (*Nexmif* $^{+/-}$) female mouse model. Female *Nexmif* $^{\pm}$ mice demonstrate representative ASD-like behavioral phenotypes including reduced social interactions, repetitive behaviors, and impaired memory, but with intact development of communication. *Nexmif* haploinsufficiency results in mosaic cellular expression of NEXMIF in the brains of these mice, leading to a mixed coexistence of both NEXMIF^{+} and NEXMIF^{-} neurons due to random XCI. Haploinsufficient *Nexmif* expression results in impairments in neuronal structure development, such as dendritic arborization and synaptic connectivity. These findings validate the mouse model for *NEXMIF* haploinsufficiency ASD and provide new insights into our understanding of the role of *NEXMIF* in brain development and the pathobiological mechanisms underlying *NEXMIF* ASD in females.

2. Materials and METHODS

2.1. Animal care and use

All procedures involving the use of animals were in line with the policies of the Institutional Animal Care and Use Committee (IACUC PROTO201800574: 17–022) at Boston University. Mouse colonies (C57BL/6 J genetic background) were maintained in the Boston University Laboratory Animal Care Facility (LACF) on the Charles River Campus. Heterozygous *Nexmif* female mice were crossed with wildtype (WT) male mice, and the heterozygous female mice were used in experiments. All of the WT (*Nexmif* $^{+/+}$) mice were randomized female littermate controls of the heterozygous mice (*Nexmif* $^{+/-}$). Adult mice were used in the behavioral studies to avoid variability due to changes during adolescence. Transgenic mice were backcrossed to C57 B l/6 J mice >10 times prior to use.

2.2. Genotyping

DNA was isolated from tail snips for genotyping using the Hot Shot Method. A 2 mm tail snip was collected from each mouse at the time of weaning on postnatal day 21 (P21) and placed in a 1 mL tube. Tail snips were incubated for 30 min at 95 °C in 75 μl of alkaline lysis buffer (25 mM NaOH, 0.2 M EDTA). The tubes were cooled to room temperature for 5 min before 75 μl of neutralization buffer (40 mM Tris-HCl, pH 5) was added. The tubes were vortexed to mix and 1 μl of DNA extract was used in the following PCR protocol run

on a Biorad DNA engine Tetrad 2 Peltier Thermal Cycler.

	Initial Denaturation	94 °C	5 min
30 cycles {	Denature	98 °C	15 s
	Anneal	55 °C (WT) or 59 °C (KO)	30 s
	Extend	72 °C	1 min
	Final Extension	72 °C	5 min
	Hold	4 °C	∞

The resulting PCR fragments were run on a 1 % agarose gel with ethidium bromide to stain and visualize DNA under UV light. Two sets of primers were used to genotype NEXMIF Heterozygous mice. One set (WT) was targeted against the deleted exon 4 region using the primers: 5′-AGGACTTGCTTAGGTTGCTTCATGGAA−3′ and 5′-CTTAAATTGCTCTACCTCAA GACCACCA−3′ with an expected PCR fragment of 949 bp. The other set (KO) was targeted against the KO sequence using the primers: 5'−CACACCTCCCCCTGAACCTGAAAG −3′ and 5'−CCCACGAAGGGATCATACCCTGTA−3′ with an expected PCR fragment of 794 bp. Prior to mouse primary neuron culture (described below), tail snips were collected from P0–P1 mice to determine their sex and genotype. The sex-specific primers used target the DEAD-box Y RNA helicase DBY (DDX3Y) gene, which is specific to males: 5′-GAAGTAGCCGTGGACGTTCT-3′ and 5′-GCCAAGGTTTGCTTGTAGCC-3′ with an expected PCR fragment of 618 bp. The presence of this fragment in each DNA sample indicates the male sex, while the absence of this fragment indicates the female sex.

2.3. Three-chamber social test

A three-chambered box measuring 65 × 28 × 28 cm was constructed from 0.75 in. white plastic board with 4 × 4 in. cut-out doors in the walls to the center chamber allowing movement between chambers. A small wire cage was placed in each of the side chambers to later house stranger mice. Three days before the test, mice were habituated to the three-chambered box with empty cages in both of the side chambers and allowed to move freely between all three chambers for 5 min each day. On the testing day, the side doors were blocked with white plastic boards and the test mouse was placed into the center chamber with a stranger WT mouse (Mouse 1) placed under the wire cage in either of the side chambers. Once the doors were unblocked, the test mouse was allowed to move freely within the apparatus for 5 min. Afterwards, the test mouse was immediately returned to the center chamber, the doors were blocked again, and a second mouse (Novel Mouse) was placed in the wire cage of the other side chamber. The center doors were unblocked again and the test mouse was allowed to move freely within the apparatus for another 5 min. Between test mice, the entire apparatus was wiped with 70 % ethanol to eliminate odor cues. Animals' movement was analyzed for the time spent interacting with each mouse or empty cage (nose $\leq$2 cm) and the time spent in each chamber.

2.4. Marble burying test

The marble burying was conducted in a square plastic bin with a 3 in. layer of fresh pine bedding. Twenty-five glass marbles (0.25 in. diameter) were arranged in a 5 × 5 grid on top of the bedding. The mouse was placed into the bin and allowed to freely move and bury marbles for 30 min. The number of marbles buried after 5, 10, 15, 25 and 30 min were manually counted.

2.5. Grooming test

Grooming was assessed in the home cage with a 3 in. layer of fresh pine bedding. Mice were singly placed back into the cage and allowed to move freely for 20 min. Video recordings were captured from the side of the cage. The amount of time spent grooming and the number of grooming instances were manually quantified.

2.6. Open field test

The open field test was performed in a 0.75 in. thick white plastic box with a base measuring 28 × 28 × 28 cm. Lights in the testing room were dimmed for comfort of the animal with only a small desk lamp in the corner for the experimenter. The mouse was habituated to the testing room for 3 days and handled for 5 min each session. On the test day, each mouse was placed into the center of the box and allowed to explore the chamber for 15 min. Animal movement was analyzed for movement speed, entries to the open center, and track lengths.

2.7. Barnes Maze spatial memory test

The Barnes maze consisted of a 48 in. diameter, 0.75 in. thick, circular white board with twenty holes (2 in. diameter) evenly distributed around the board 1 in. from the edge. The maze was mounted 30 in. above the ground on a pedestal that allowed it to rotate from the center. A plain curtain with a few shapes attached as spatial cues surrounded the maze to simplify the cues for the mice. The escape cage beneath the escape hole consisted of a black plastic box with a ramp to allow for easy access.

During each session, each mouse was placed in the center of the maze under an opaque container. The aversive stimuli of four bright ceiling lamps and a loud alarm were turned on when the mouse was released from the container and allowed to roam freely

about the maze. The ceiling lights and loud noise were on while the mouse explored the maze, but were turned off immediately after the mouse entered the escape hole. The maze and escape cage were cleaned with 70 % ethanol between test sessions to avoid olfactory cues, and the maze was randomly rotated after each mouse to avoid intra-maze odor or visual cues. The escape hole remained in the same location relative to the spatial cues.

On day 1 of the procedure, the mice were habituated to the maze. After 3 min of exploring the maze, the mouse was gently nudged into the escape hole. The mouse was allowed to stay in the escape hole without aversive stimuli for 2 min. All mice were adapted to the maze in this way. On days 2–5, the mice underwent training 3 times each day (12 times total) to learn to enter the escape hole on their own and to ensure a strong memory for the location of the escape hole. For each training trial, if the mice did not enter the escape hole on their own after 3 min, they were gently nudged into the hole. After the mice entered the escape hole, the aversive stimuli were turned off and the mice remained in the escape chamber for 1 min. On days 6 and 10 (1 d and 5 d post-training), the mice were tested for their memory of the escape hole location. During the memory probes, the escape hole was covered, and the mouse was allowed to freely roam for 3 min. Recordings of animal movement were analyzed to test the spatial memory of the mice. Primary latency to the escape hole, distance traveled to the escape hole, percentage of erroneous nose pokes, and time spent in each quadrant of the maze were quantified.

2.8. Ultrasonic vocalization recording

Ultrasonic vocalizations (USVs) were recorded from mouse pups at P5, P7, and P9 using a CM16/CMPA microphone (Avisoft Bioacoustics, Berlin, Germany). Briefly, a pup was separated from their dam and littermates to illicit calling and then isolated in a recording chamber with the microphone 15 cm above the chamber. Between each pup, the recording chamber was cleaned with 70 % ethanol and dried. The pups were recorded for 5 min in a 16-bit format at a sampling rate of 300 kHz. The microphone was connected to a pre-amplifier UltraSoundGate 116 H b (Avisoft Bioacoustics, Berlin, Germany) and the digitized sonograms were stored in a computer. All of the recordings were analyzed using SASLab Pro 5.2.12 (Avisoft Bioacoustics, Berlin, Germany). The spectrograms were first generated using a fast Fourier transform (FlatTop window, 256 FFT length, 50 % window overlap, and a 100 % frame), followed by high-pass filtering of the transformed spectrograms to eliminate any background noise below 30 kHz. The USVs were manually labeled and classified by two independent investigators. The number of calls, the total time spent calling, the mean call duration, and the peak frequency and amplitude were measured. The calls were classified into the following groups based on their acoustic features; simple: short, flat, upward, downward, chevron, U shape, and complex: modulated, frequency jump, multiple jumps, harmonic.

3. Immunocytochemistry of cultured neurons

Cortical or hippocampal neurons were fixed in a 4 % paraformaldehyde/4 % sucrose solution at room temperature (RT) for 8 min. Cell membranes were permeabilized in 0.3 % Triton-X-100 (Fisher Biotech) in phosphate buffered saline (PBS) for 5 min and then washed three times in PBS. Cells were blocked in 10 % goat serum in PBS at RT for 1 h. Following blocking, the cells were incubated in primary antibodies (5 % goat serum in PBS) at RT for 2 h, washed three times with PBS, and incubated with Alexa Fluor-conjugated fluorescent secondary antibodies (1:500, Life Technologies) for 1 h at RT. Cells were washed three times with PBS, stained with Hoescht (1:10,000, Thermo Fisher) to label the nuclei, and mounted to glass slides with Prolong Gold anti-fade mounting reagent (Life Technologies) for subsequent microscopy. The mounted coverslips were kept in the dark at RT overnight prior to imaging.

4. Immunohistochemistry of brain slices

Adult mice were transcardially perfused with cold PBS prior to collection of the brain. Brains were fixed for 4–6 h in 4 % paraformaldehyde and placed in a 30 % sucrose/PBS solution as a method for cryoprotection. Brains were placed in molds to be rapidly frozen in OCT (Tissue-Tek) and stored at −80 °C until they were sliced into 20 μm sections using the LEICA CM1850 cryostat (LEICA Biosystems). The sections were mounted onto SuperFrost microscope slides (Fisher Scientific) and stored at −20 °C until staining. To prepare for immunostaining, sections were hydrated in PBS for at least 2 h and were subjected to antigen retrieval. Briefly, sections were microwaved in sodium citrate buffer (10 mM, pH 6) at 800 W for 1 min followed by 80 W for 10 min. The sections were then cooled to RT for 20 min and then blocked in 10 % goat serum, 0.3 % Triton X-100/PBS for 1 h. Sections were then incubated in primary antibodies (5 % goat serum PBS) overnight at 4 °C, washed three times with PBS, and incubated in Alexa Fluor-conjugated fluorescent secondary antibodies (1:500, Life Technologies) for 1 h at RT. The brain slices were washed three times with PBS, stained with Hoescht (1:10,000, Thermo Fisher) to label the nuclei, and mounted under a coverslip with Prolong Gold anti-fade mounting reagent (Life Technologies). Slides were then allowed to dry overnight at room temperature and stored at −20 °C for subsequent visualization.

4.1. Golgi staining

Whole brains from adult WT and *Nexmif* Heterozygous female mice were subjected to Golgi neuron staining using the FD Rapid GolgiStain Kit (FD Neurotechnologies, catalog #PK401) according to the manufacturer's instructions. Mice were sacrificed in a 4 % CO_2 chamber, and the brains were then collected and washed in cold PBS. The brains were submerged in a Golgi-Cox solution that contained mercuric chloride, potassium dichromate, and potassium chromate. The solution was replaced following 1 d of immersion with fresh solution and stored at RT in the dark for 2 weeks. After immersion, the brains were rapidly frozen and stored at −80 °C prior

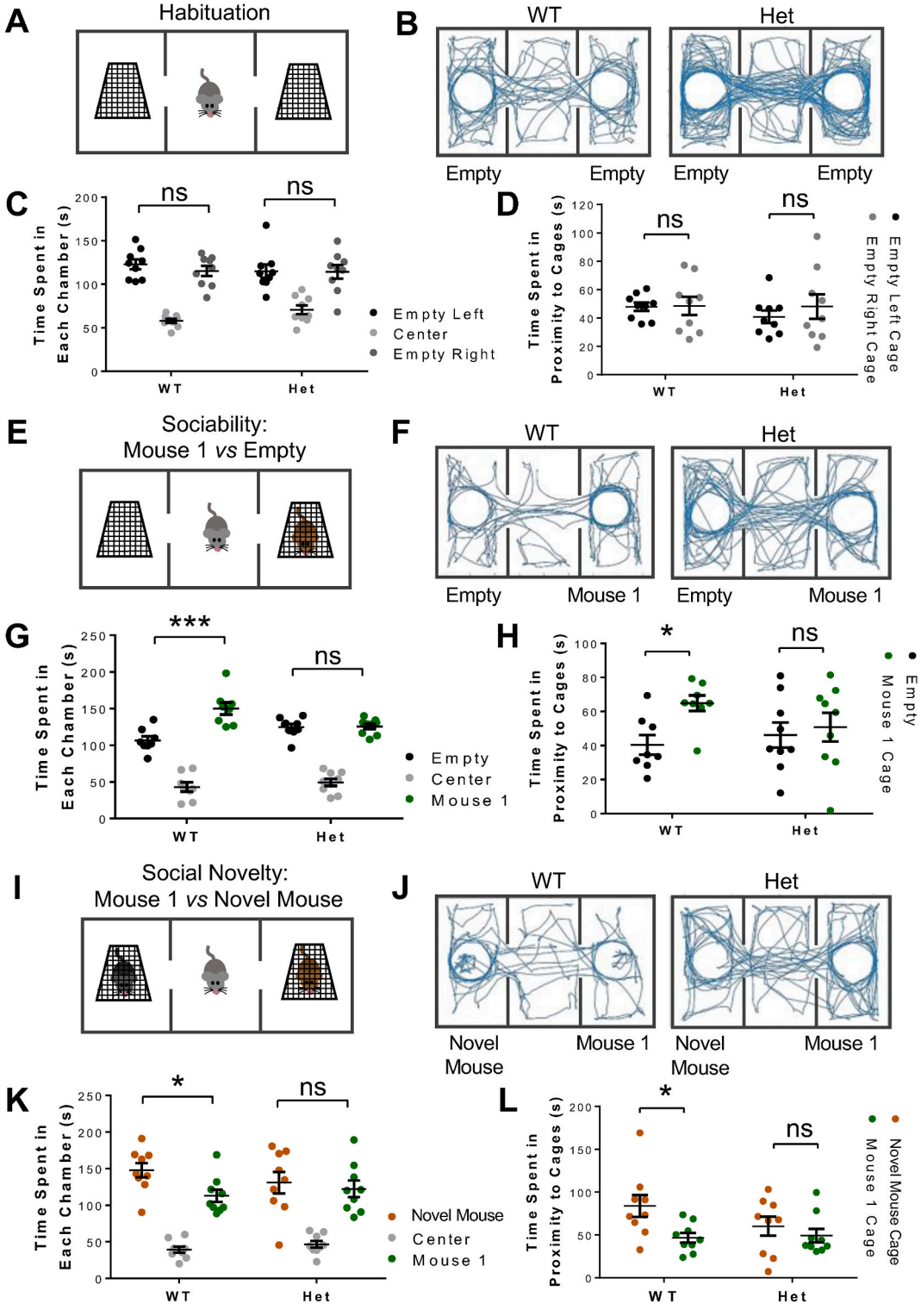

(caption on next page)

Fig. 1. ***Nexmif*** **heterozygous mice show abnormalities in social behaviors (A)** Habituation to the three-chamber apparatus. Mice were released from the center chamber, with empty cages in the adjacent chambers, and allowed to move freely within the apparatus for 5 min each session for 3 d prior to beginning the sociability and social novelty tests. **(B)** Representative traces of animal track paths in the habituation phase for WT and *Nexmif* $^{\pm}$ mice. **(C, D)** Neither WT nor *Nexmif* $^{\pm}$ animals showed preference for either side chamber (C) (Left vs Right: WT: $t_{(32)} = 0.7979$, KO: $t_{(32)} = 0.0977$; $F_{(1,\ 32)} = 0.401$, $p = 0.5311$) or either empty cage (D) (Left vs Right: WT: $t_{(32)} = 0.059$, KO: $t_{(32)} = 0.849$; $F_{(1,\ 32)} = 0.4129$, $p = 0.5251$) during habituation. **(E)** Paradigm for the sociability test. An unfamiliar mouse (Mouse 1) was placed into either of the side chambers and the test mouse was allowed to move freely within the apparatus. **(F)** Representative traces of animal track paths in the sociability test for WT and *Nexmif* $^{\pm}$ mice. **(G, H)** Het mice failed to demonstrate the sociability observed in WT mice, which show an increase in the time spent in the chamber (G) (Empty vs Mouse 1: WT: $t_{(30)} = 5.354$, KO: $t_{(30)} = 0.1375$; $F_{(1,\ 30)} = 15.92$, $p = 0.0004$) and in proximity to the cage (H) (Empty vs Mouse 1: WT: $t_{(30)} = 2.452$, KO: $t_{(30)} = 0.4959$; $F_{(1,\ 30)} = 4.514$, $p = 0.042$) with Mouse 1. **(I)** Paradigm for the social novelty test. A second mouse (Novel Mouse) was placed into the remaining empty chamber opposite to Mouse 1, and the test mouse was allowed to interact with both mice. **(J)** Representative traces of animal track paths in the social novelty test for WT and *Nexmif* $^{\pm}$ mice. **(K, L)** WT mice showed an increase in the time spent in the chamber (K) (Mouse 1 vs Novel Mouse: WT: $t_{(30)} = 3.145$, KO: $t_{(30)} = 0.5769$; $F_{(1,\ 30)} = 7.205$, $p = 0.0117$) and in proximity to the cage (L) (Mouse 1 vs Novel Mouse: WT: $t_{(30)} = 2.818$, KO: $t_{(30)} = 1.591$; $F_{(1,\ 30)} = 9.526$, $p = 0.0043$) with the Novel Mouse, but the *Nexmif* $^{\pm}$ mice failed to demonstrate the preference for social novelty. Het, *Nexmif* $^{+/-}$. $n = 9$ mice/group. $^{*}p < 0.05$, $^{**}p < 0.01$, ns = not significant. Error bars represent the standard error of the mean (SEM).

to slicing. The brain slices were then sliced coronally on a cryostat at 100 μm thickness and were mounted on gelatin-coated slices (FD Neurotechnologies, catalog #PO101) and air dried at RT before further processing. Sections were then rinsed in distilled water, incubated in staining solution for 10 min, and dehydrated with 50 %, 75 %, 95 %, and 100 % ethanol. Xylene was then used to defat the sections, prior to the sections being mounted onto coverslips with Permount mounting medium (Thermo Fisher Scientific). The sections were then stored at RT in the dark for subsequent visualization.

4.2. Sholl analysis

Complexity of dendritic arborization was quantified using IMARIS 9.5.1 (Bitplane AG, Zurich, Switzerland). The dendrites of each neuron were manually traced using the Filament Tracer AutoPath protocol. The tracings were used to obtain measurements of the total dendritic length, mean dendritic length, and dendritic complexity evaluated by Sholl analysis. Sholl analysis within IMARIS measured dendritic branching complexity by counting the number of intersections between the dendritic filaments and concentric circles set at 1 μm intervals from the soma. The Sholl value at each radius was then plotted versus the radius of its intersecting circle.

4.3. Primary neuron culture

Cortical and hippocampal brain tissue were collected from the brains of P0–P1 *Nexmif* Het mice and WT littermate controls and used for primary neuron culture. The sex and genotype of each P0–P1 mouse were determined via PCR prior to culturing (described above). Each brain region was individually digested in papain (1 mg/ml in Hanks balanced salt solution, Sigma-Aldrich; cat. # 4762) for 20 min at 37 °C, and triturated in a trituration buffer [0.1 % DNase (cat. # PA5-22017 RRID: AB_11153259), 1 % ovomucoid (Sigma-Aldrich; cat. #T2011)/1 % bovine serum albumin (Sigma-Aldrich; cat. #05470) in Dulbecco's modified Eagle's medium] to fully dissociate the neurons. The dissociated neurons were then manually counted and plated on circular coverslips (18-mm; Carolina, Burlington, NC; cat. # 633013, No. 0) in 60-mm Petri dishes (five coverslips/dish) that were coated overnight at 37 °C in poly-L-lysine (Sigma-Aldrich; cat. #P2636; 100 μg/ml in borate buffer), and then rinsed three times with autoclaved deionized water, and placed in plating medium [minimal essential medium (500 mL) containing 10 % fetal bovine serum (Atlanta Biologicals, Flowery Branch, GA; cat. #S11550), 5 % horse serum (Atlanta Biologicals; cat. #S12150), 31 mg l-cysteine, 1 % penicillin/streptomycin (Corning, Corning, NY; cat. # 30-002-Cl), and L-glutamine (Corning; cat. # 25-005-Cl) prior to cell plating. 24 hr after plating, the plating medium was removed and replaced by feeding medium (neurobasal medium supplemented with 1 % horse serum, 2 % NeuroCult SM1 supplement, and 1 % penicillin/streptomycin and L-glutamine). After 7 d in vitro, the feeding medium was supplemented with 5′-fluoro-2′-deoxyuridine (10 μm; Sigma-Aldrich; cat. #F0503) to suppress glial growth.

4.4. Microscopy

The fluorescence exposure time was manually adjusted so that the signals were within the full dynamic range. Once the proper parameters were obtained, they were set and used throughout image acquisition for the experiment. Both the histogram and glow scale look-up table were used to monitor saturation level of the images.

For ICC: Fluorescent images were taken with a 40× air-objective (numerical aperture, 0.95) on a DS-Fi2 Color Camera on a Nikon Eclipse NiE using NIS-Elements software. All neuron images were processed and analyzed using the free NIH ImageJ software.

For IHC: Images of brain sections were taken with 10x and 20× air-objectives using a Nikon C2+ Si spectral laser scanning confocal microscope using NIS-Elements software.

For Golgi staining: images were acquired using brightfield transmitted light with a 40× air-objective (numerical aperture, 0.95) on a DS-Qi1 Monochrome Cooled Digital Camera on a Nikon Eclipse NiE using NIS-Elements software. Each neuron was scanned by changing the depth of the Z plane to ensure that the dendrites, as well as all parts of the cell, were intact. Basal spine number on neurons was measured with ImageJ software.

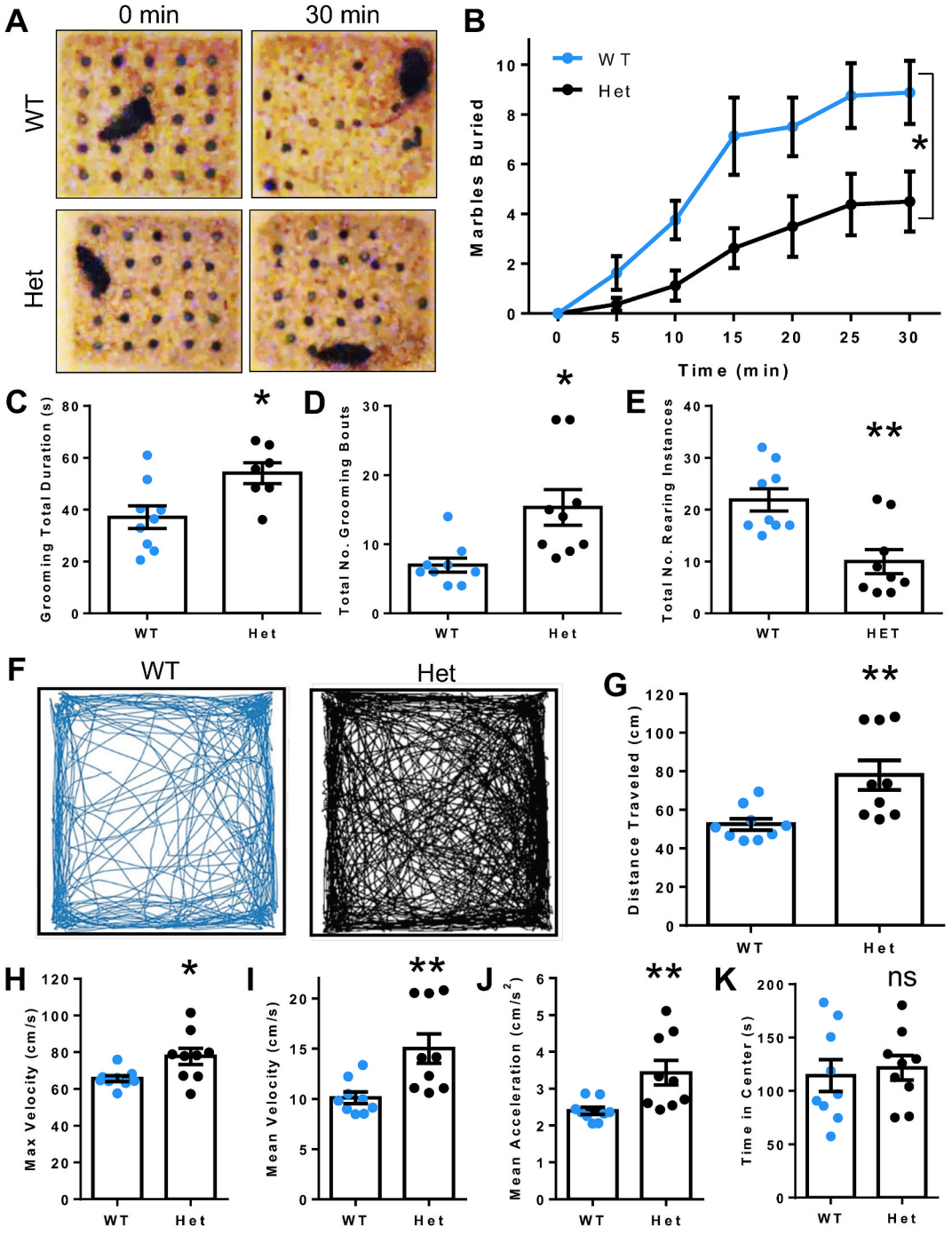

Fig. 2. ***Nexmif*** **heterozygous mice display aberrant marble burying behavior, increased repetitive grooming, and hyperactivity (A, B)** In the marble burying test, *Nexmif* $^{\pm}$ animals buried significantly fewer marbles (repeated measures two-way ANOVA followed by Bonferroni's multiple comparison test; $F_{(1,14)} = 7.924$, $p = 0.0138$ between genotypes; $F_{(6,\ 84)} = 31.02$, $p < 0.0001$ between time points). **(C, D)** *Nexmif* $^{\pm}$ mice spent an increased amount of time grooming (C) ($t_{(14)} = 2.786$, $p = 0.0146$) and performed an increased number of grooming episodes (D) ($t_{(16)} = 3.021$, $p = 0.0081$). **(E)** *Nexmif* $^{\pm}$ animals demonstrated a reduction in rearing behavior ($t_{(16)} = 3.757$, $p = 0.0017$). **(F)** Representative track paths of WT and *Nexmif* $^{\pm}$ animals in the open field test. **(G–K)** *Nexmif* $^{\pm}$ animals showed increased track lengths (G) ($t_{(16)} = 3.132$, $p = 0.0064$), increased max (H) ($t_{(16)} = 2.560$, $p = 0.0210$) and mean (I) ($t_{(16)} = 3.132$, $p = 0.0064$) speeds, increased mean acceleration (J) ($t_{(16)} = 2.966$, $p = 0.0091$), and no change in time spent in the central area (K) ($t_{(16)} = 0.3870$, $p = 0.7039$) in the open field test. $n = 9$ mice/group. $^{*}p < 0.05$, $^{**}p < 0.01$, ns = not significant. Error bars represent the SEM.

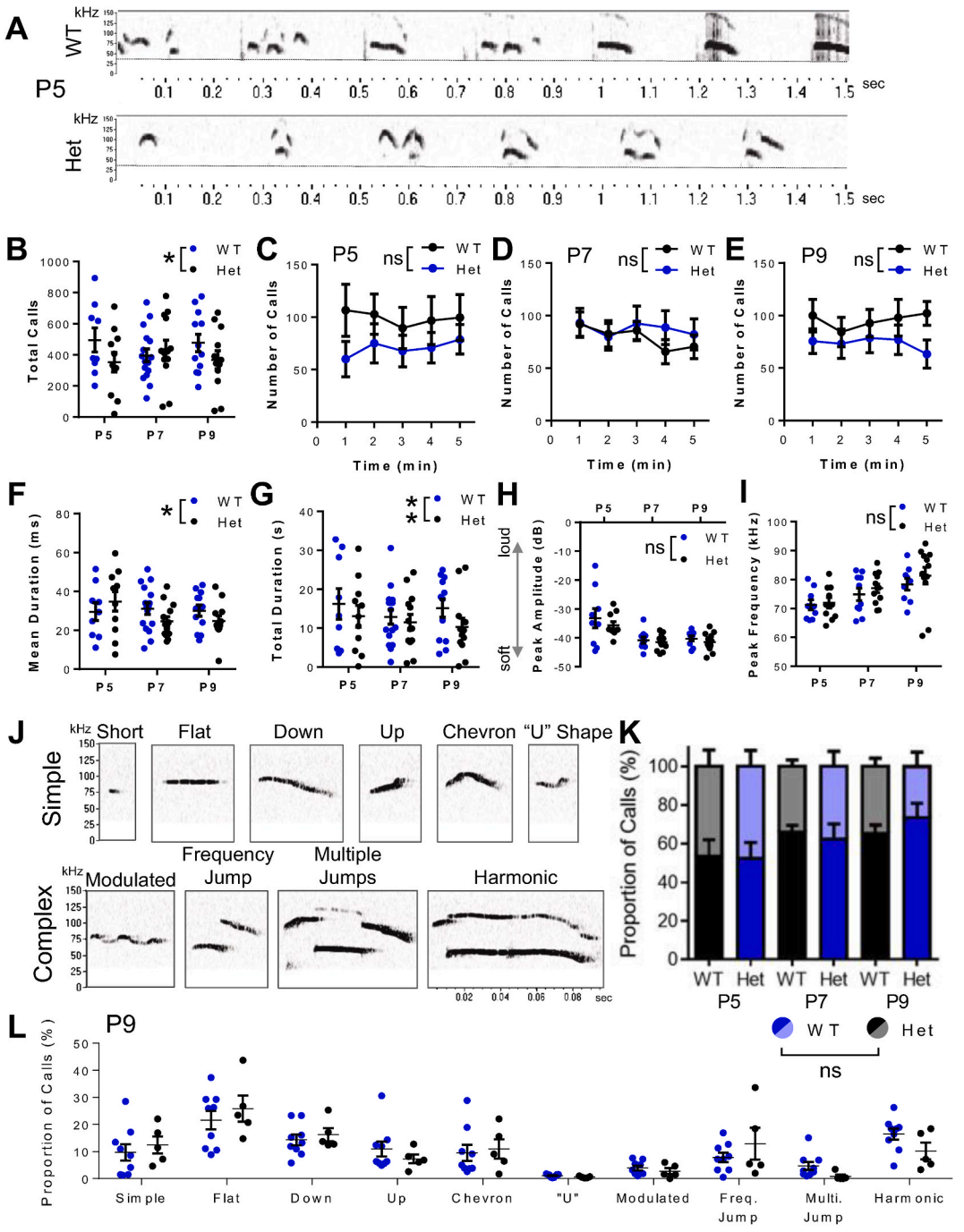

(caption on next page)

Fig. 3. *Nexmif* heterozygous mice show moderate impairment in communication behavior (A) Representative vocalizations from P5 recordings for WT and *Nexmif* $^{\pm}$ mice. Top: the raw USV signals. Bottom: the associated spectrograms; all are 1.5 s in length. Dashed line depicts the 30 kHz frequency threshold for eliminating noise. **(B)** Quantification of the number of calls made by *Nexmif* $^{\pm}$ animals compared to WT controls at each developmental time point recorded ($F_{(1,8)} = 5.959$, $p = 0.0405$ between genotypes (P5); $F_{(2,16)} = 0.2021$, $p = 0.8191$ between time points). **(C–E)** Mean number of calls emitted across the 5 min recording period at each developmental time point P5 (C) ($F_{(1,8)} = 0.7084$, $p = 0.4244$ between genotypes; $F_{(4,32)} = 0.1688$, $p = 0.9527$ between time points), P7 (D) ($F_{(1,12)} = 0.1227$, $p = 0.7322$ between genotypes; $F_{(4,48)} = 1.353$, $p = 0.2643$ between time points), and P9 (E) ($F_{(1,11)} = 4.040$, $p = 0.0696$ between genotypes; $F_{(4,44)} = 0.3459$, $p = 0.8454$ between time points). **(F–G)** Quantification of the mean call syllable duration (F) ($F_{(1,8)} = 6.381$, $p = 0.0355$ between genotypes (P7); $F_{(2,16)} = 0.8940$, $p = 0.4285$ between time points) and the total time spent calling (G) ($F_{(1,8)} = 14.28$, $p = 0.0054$ between genotypes (P9); $F_{(2,16)} = 0.4545$, $p = 0.6427$ between time points) between WT and *Nexmif* $^{\pm}$ mice. **(H–I)** *Nexmif* $^{\pm}$ mice showed no change in peak amplitude of calls (H) ($F_{(1,8)} = 2.214$, $p = 0.1751$ between genotypes; $F_{(2,16)} = 9.698$, $p = 0.0017$ between time points), or peak frequency of calls (I) ($F_{(1,8)} = 0.1464$, $p = 0.7120$ between genotypes; $F_{(2,16)} = 1.721$, $p = 0.2104$ between time points) at any time point. **(J)** Representative calls of each type used in syllable characterization. **(K)** WT and *Nexmif* $^{\pm}$ mice showed similar ratios of Simple vs Complex call types at each time point ($F_{(1,84)} = 0.0182$, $p = 0.8931$). **(L)** *Nexmif* $^{\pm}$ animals showed no change in frequency of particular call syllable types compared to WT animals at P9 (Simple: $t_{(12)} = 0.584$, $p = 0.570$; Flat: $t_{(12)} = 0.733$, $p = 0.478$; Down: $t_{(12)} = 0.606$, $p = 0.556$; Up: $t_{(12)} = 0.927$, $p = 0.372$; Chevron: $t_{(12)} = 0.295$, $p = 0.773$; "U": $t_{(12)} = 1.90$, $p = 0.0824$; Modulated: $t_{(12)} = 0.829$, $p = 0.423$; Freq. Jump: $t_{(12)} = 1.04$, $p = 0.318$; Multi. Jump: $t_{(12)} = 1.86$, $p = 0.0874$; Harmonic: $t_{(12)} = 1.76$, $p = 0.104$). $n = 9$–16 animals. ns = not significant. Error bars represent the SEM.

4.5. Statistical analysis

For ICC: Synaptic puncta and spine density were analyzed using NIH FIJI (ImageJ) Software. Measurements from at least three segments of secondary dendrites from different neurites were analyzed to represent one neuron.

For IHC: Mosaic expression of NEXMIF in brain slices was analyzed using the Spots protocol in IMARIS 9.5.1 (Bitplane AG, Zurich, Switzerland). Images underwent deconvolution according to the parameters of the microscope objective used for capture. Neurons were identified and labeled based on NeuN expression. Neurons were then sorted as NEXMIF+ and NEXMIF- based on NEXMIF expression.

For behavioral tests: Behavioral tests were recorded and captured with a Logitech c920 webcam during each test. Locomotion tracks were generated using idtracker.ai software [31]. These tracks were used in custom scripts written in Python to quantify the desired aspects of the animals' movement. The same animals were used in all the behavioral tests and therefore were not randomly assigned. Investigators were not blinded to the genotypes.

Statistical analysis was performed using the two-population student's *t*-test, one-way ANOVA with Tukey post-hoc test, or repeated measures two-way ANOVA with Sidak's multiple comparison test as appropriate. All data are expressed as mean ± standard error of the mean (SEM) and were analyzed using GraphPad Prism 6 statistical software (USA, GraphPad Software). The criterion for data exclusion was the Identify outliers function in Prism software using the Rout method. All data were treated as parametric for statistics. $p < 0.05$ is considered statistically significant. p values are presented as $p > 0.05$ (ns, not significant), * $p < 0.05$, ** $p < 0.01$, and *** $p < 0.001$.

5. Results

5.1. *Nexmif* $^{\pm}$ *mice demonstrate autistic-like features in social behavior*

Individuals with ASD-causing *NEXMIF* variants present with autistic behaviors, poor to absent speech, ID, and often epilepsy [16,17,20,22,24]. Additionally, *Nexmif* $^{-/y}$ KO mice demonstrate decreased sociability, reduced communication, increased repetitive behaviors, and impaired spatial memory [26]. We thus sought to characterize the extent of behavioral changes that result from *Nexmif* haploinsufficiency. We first examined the social behavior of the *Nexmif* $^{\pm}$ mice using the three-chamber test, which assesses general sociability and preference for social novelty [32]. Animals were habituated to the three-chambered apparatus before testing by letting them explore all three areas (Fig. 1A). Neither female WT nor female *Nexmif* $^{\pm}$ mice showed a preference for a particular side of the testing apparatus (Fig. 1B–D). For the sociability test, an unfamiliar female mouse (Mouse 1) was placed into a cage in one of the side chambers and the test mouse was allowed to move throughout the three-chambers (Fig. 1E). WT mice spent a significant amount of time investigating and interacting with Mouse 1 relative to the empty chamber; however, *Nexmif* $^{\pm}$ mice failed to show a preference toward Mouse 1 in either the amount of time spent in the chamber of Mouse 1 or in close proximity to the cage housing Mouse 1 (Fig. 1F–H), indicating *Nexmif* $^{\pm}$ mice have impairments in sociability. We then tested animals for preference for social novelty by placing a second unfamiliar female mouse (Novel Mouse) into the remaining empty cage in the other side chamber and allowing the test mouse to roam freely (Fig. 1I). *Nexmif* $^{\pm}$ mice showed no preference toward the Novel mouse (Fig. 1J) as demonstrated by similar times spent in either side chamber (Fig. 1K) and in close proximity to either mouse's cage (Fig. 1L), whereas the WT mice spent significantly more time in the side chamber with the Novel mouse (Fig. 1K) and in close proximity to the Novel mouse's cage (Fig. 1L). These findings indicate that the *Nexmif* $^{\pm}$ mice have a lack of interest in social novelty.

5.2. *Increased repetitive behavior and hyperactivity in Nexmif* $^{\pm}$ *mice*

We further investigated changes in the behavior of *Nexmif* $^{\pm}$ mice using the marble burying test. We placed WT and *Nexmif* $^{\pm}$ mice in

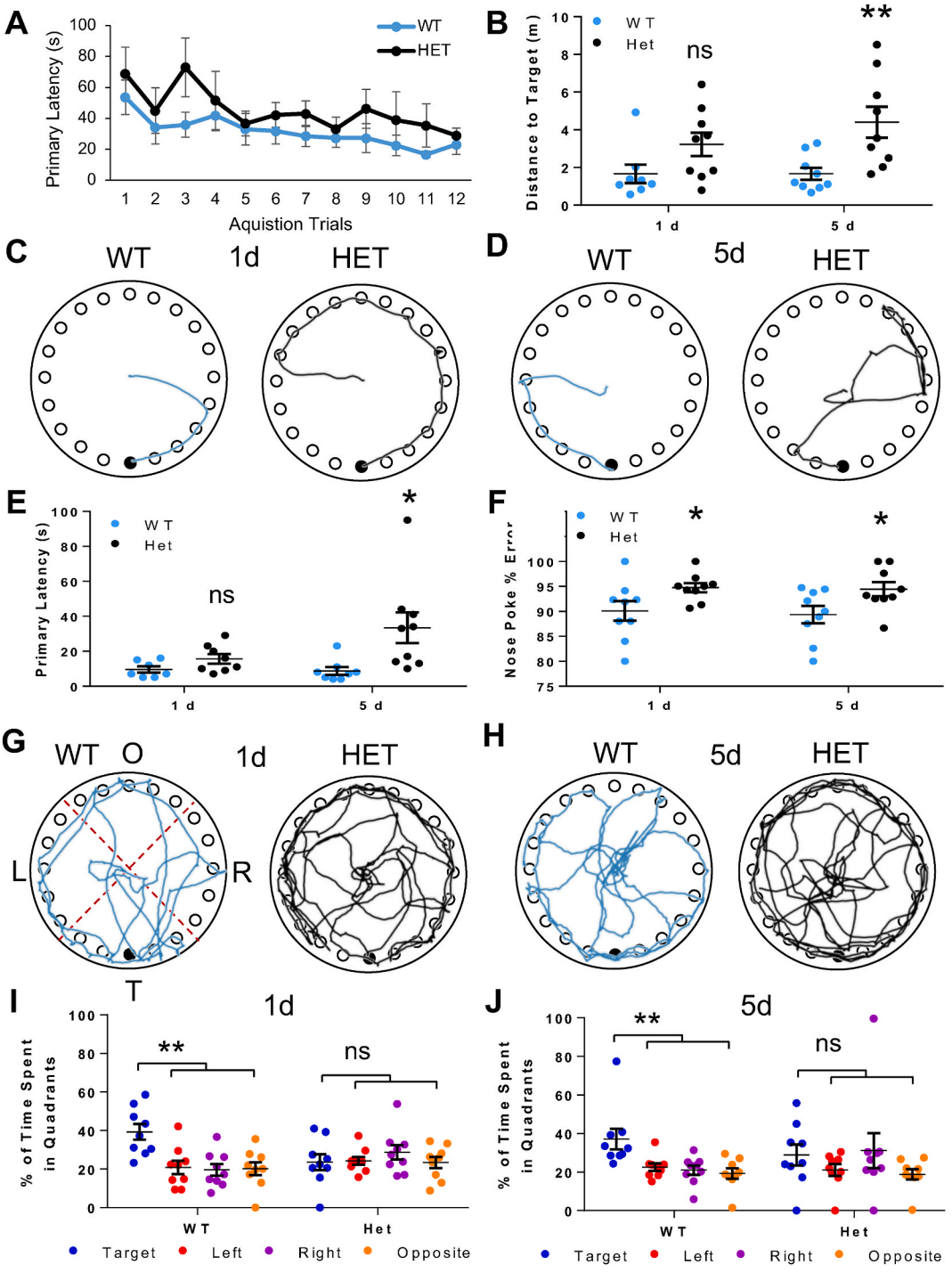

(caption on next page)

Fig. 4. *Nexmif* heterozygous mice display defects in learning and memory in the Barnes maze test **(A)** Quantification of the primary latency (s) to find the target hole across all training trials (3 trials per day over 4 days) for WT and *Nexmif* $^{\pm}$ animals. **(B)** Total track length distance before initial contact with target hole was increased in *Nexmif* $^{\pm}$ mice 5 d after training ($F_{(1,7)} = 15.63$, $p = 0.0055$ between genotypes; $F_{(1,7)} = 3.519$, $p = 0.1028$ between time points). **(C, D)** Representative traces of track paths to initial contact with target in the Barnes spatial memory maze during the 1 d (C) and 5 d (D) memory probe for WT and *Nexmif* $^{\pm}$ animals. **(E)** Primary latency to the target hole was increased in the *NEXMIF* $^{\pm}$ animals in the test 5 d after training ($F_{(1,7)} = 7.828$, $p = 0.0266$ between genotypes; $F_{(1,7)} = 0.7161$, $p = 0.4254$ between time points). **(F)** *Nexmif* $^{\pm}$ mice made a significantly higher number of nose poke errors in both the 1 d and 5 d memory tests than WT mice ($F_{(1,8)} = 11.35$, $p = 0.0098$ between genotypes; $F_{(1,8)} = 0.2212$, $p = 0.6507$ between time points). **(G, H)** Representative traces of track paths over 3 min test in the Barnes spatial memory maze during the 1 d (G) and 5 d (H) memory probe for WT and *Nexmif* $^{\pm}$ animals. T, target; L, left; R, right; O, opposite. **(I, J)** *NEXMIF* $^{\pm}$ mice did not spend significantly more time in the target quadrant compared to the other maze quadrants, as WT controls do, in the tests at 1 d (I) (WT: Target v Left: $t_{(64)} = 3.810$, Target v Right: $t_{(64)} = 4.088$, Target v Opposite: $t_{(64)} = 3.967$; Het: Target v Left: $t_{(64)} = 0.1492$, Target v Right: $t_{(64)} = 1.050$, Target v Opposite: $t_{(64)} = 0.0424$; $F_{(3,\ 64)} = 3.347$, $p = 0.0244$) and 5 d (J) (WT: Target v Left: $t_{(64)} = 2.218$, Target v Right: $t_{(64)} = 2.442$, Target v Opposite: $t_{(64)} = 2.716$; Het: Target v Left: $t_{(64)} = 1.182$, Target v Right: $t_{(64)} = 0.3385$, Target v Opposite: $t_{(64)} = 1.524$; $F_{(3,\ 64)} = 3.41$, $p = 0.0227$) after training. $n = 9$ mice/group. $^{*}p < 0.05$, $^{**}p < 0.01$, ns = not significant. Error bars represent the SEM.

a square cage with 25 evenly spaced marbles on top of fresh bedding. Over 30 min, the WT animals began to bury the marbles under the bedding with a digging behavior (Fig. 2A). The *Nexmif* $^{\pm}$ animals however, buried significantly fewer marbles at all time-points after the first 10 min of observation (Fig. 2B). This finding is consistent with the reduced marble burying we observed in the *Nexmif* $^{-/y}$ KO male mice [26] and with previous reports showing decreased burying in ASD mice [33–47].

In our previous study, we found that the male *Nexmif* $^{-/y}$ mice perform excessive self-grooming [26]. This repetitive behavior has been observed in ASD and is linked to anxiety [48]. We therefore assessed the grooming behavior in the *Nexmif* $^{\pm}$ females. Similar to the *Nexmif* $^{-/y}$ males, we found that *Nexmif* $^{\pm}$ females spent a significantly longer time grooming with a significantly greater number of grooming episodes (Fig. 2C and D). We also investigated the rearing behavior of the mice, which has been linked to anxiety with increases in unsupported rearing indicating reduced anxiety [49]. We quantified unsupported rearing as the number of instances in which the mice reared up onto their hind legs without leaning on the wall of the cage. *Nexmif* $^{\pm}$ mice performed significantly fewer rearing instances than the WT controls (Fig. 2E).

We next examined the *Nexmif* $^{\pm}$ mice in the open field test. Consistent with the hyperactivity observed in *Nexmif* $^{-/y}$ males, *Nexmif* $^{\pm}$ females had a significant increase in their movement during the open field test compared to WT females, as shown by the representative traces (Fig. 2F). Quantification of the track lengths revealed that *Nexmif* $^{\pm}$ mice traveled a further distance during the test (Fig. 2G) with a significantly greater maximum velocity, average velocity, and average acceleration (Fig. 2H–J). Further quantification revealed that there is no change in time spent in the center of the open field between WT and *Nexmif* $^{\pm}$ mice (Fig. 2K). All together, these results show that *Nexmif* $^{\pm}$ mice are hyperactive with an increased level of anxiety.

5.3. *Nexmif* $^{\pm}$ *mice show moderate changes in communication by ultrasonic vocalization*

Impaired or delayed communication is a defining phenotype in ASD [50], and indeed, both males and females with *NEXMIF* mutations have shown poor or absent speech [11,12,14–17,20,22,24]. In order to assess communication behavior in the *Nexmif* $^{\pm}$ mice, we recorded and analyzed their ultrasonic vocalizations. Wild type and *Nexmif* $^{\pm}$ female pups were separated from their dam and littermates to induce calling and vocalizations were recorded for 5 min. The same animals were tested at P5, P7, and P9. Both groups of animals made calls within the ultrasonic range as depicted in representative 1.5 s of recording at P5 (Fig. 3A). The total number of calls, the number of calls per minute, average duration of calls, total time spent calling, average peak amplitude of calls, and average peak frequency of calls (Fig. 3B–I), as well as the frequency of call types (Fig. 3J– L), were analyzed at all time points. Unlike their hemizygous KO male counterparts, which showed a dramatic reduction in ultrasonic vocalization [26], the *Nexmif* $^{\pm}$ females showed moderate communication deficits compared to that of WT controls. In line with this, it has been observed that in humans, males have a more severe language impairment than females [16,17].

5.4. *Nexmif* $^{\pm}$ *mice show impairments in spatial memory*

Intellectual disability is a comorbidity in individuals with *NEXMIF* mutations, and consistently, the *Nexmif* $^{-/y}$ KO mice show ASD-like learning and memory deficits. To test whether haploinsufficient loss of *Nexmif* is sufficient to result in this phenotype, we examined spatial memory using the Barnes maze test. Mice were trained over 4 days to use spatial cues to locate a target escape hole on a circular maze containing 20 holes around its circumference. Over the acquisition training period, the *Nexmif* $^{\pm}$ mice showed a reduction in the primary latency to the target hole, indicating their ability to learn its location (Fig. 4A). After training, the target hole was covered and the ability of the mice to remember its location was assessed both 1 d and 5 d later. *Nexmif* $^{\pm}$ mice traveled a significantly longer distance than WT mice before making an initial nose poke at the target hole in the 5 d test, but not the 1 d test (Fig. 4B), as shown by representative traces (Fig. 4C and D). *Nexmif* $^{\pm}$ mice also took a longer amount of time than WT mice to find the target hole in the 5 d test, as measured by the primary latency (Fig. 4E). Quantification of the number of investigative nose pokes at the target hole versus incorrect holes showed that *Nexmif* $^{\pm}$ mice made a significantly greater number of nose poke errors than WT mice in both the 1 d and 5 d tests (Fig. 4F). We separated the maze into four quadrants to allow quantification of the amount of time the animals spent looking for the target hole in the correct area (Fig. 4G and H). This revealed that in both the 1 d and 5 d tests *Nexmif* $^{\pm}$ mice did not spend significantly more time exploring the target quadrant of the maze as compared to the other three quadrants, in contrast to

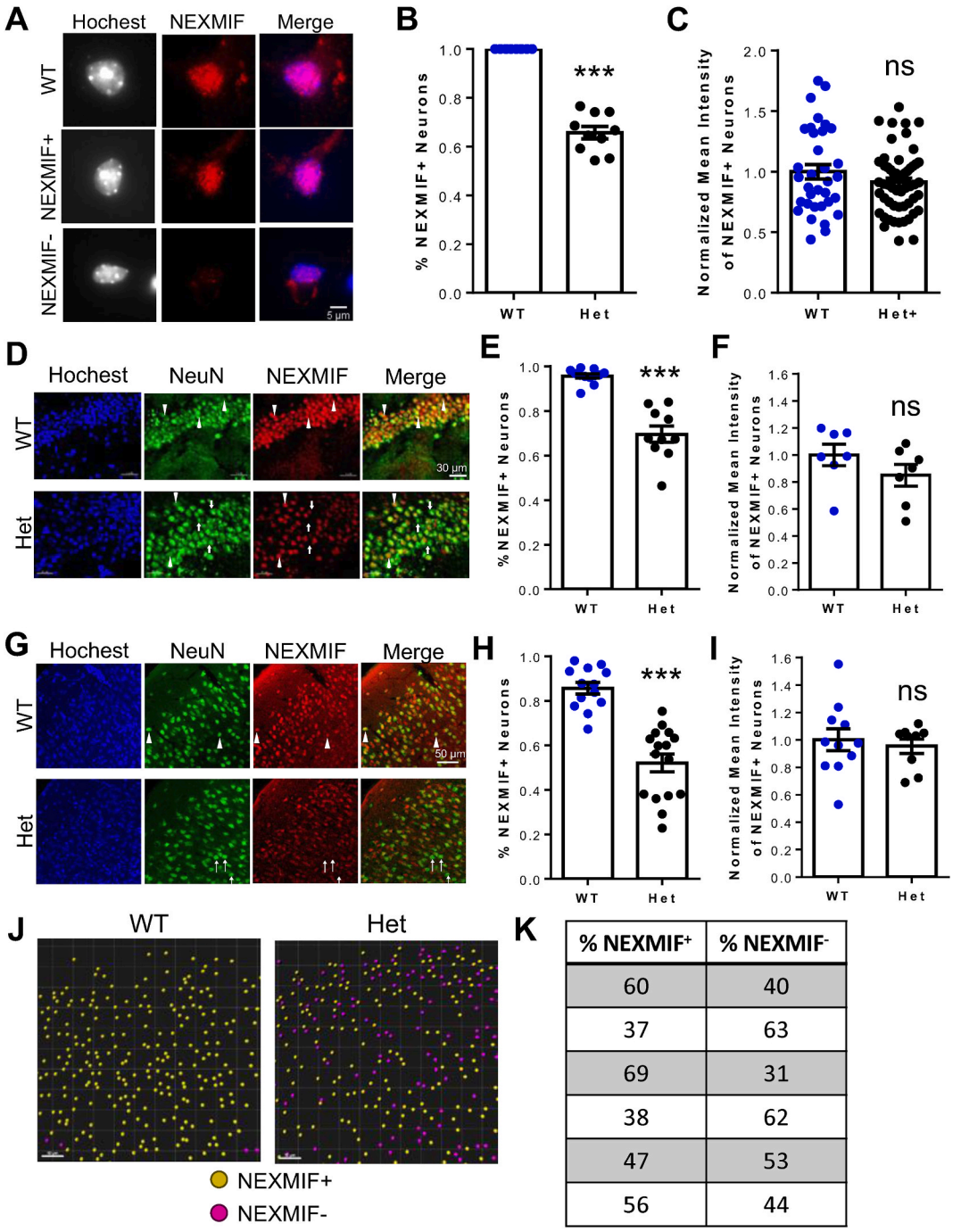

K

% NEXMIF^{+}	% NEXMIF^{-}
60	40
37	63
69	31
38	62
47	53
56	44

Fig. 5. Mosaic NEXMIF expression in the *Nexmif* heterozygous mouse (A–C) Immunostaining of NEXMIF in DIV 6 primary cortical neurons cultured from *Nexmif* WT or *Nexmif* $^{\pm}$ mouse brains shows colocalization with nuclear marker Hochest (A) and a lack of NEMXIF expression in some, but not all, neurons from *Nexmif* $^{\pm}$ brains (B) ($t_{(18)} = 13.76$, $p < 0.0001$) with no change in the level of NEXMIF in the NEXMIF^{+} neurons (C) ($t_{(90)} = 1.366$, $p = 0.1752$). Scale bar = 5 µm. $n = 10$ experiments, 30–100 cells each. **(D–I)** Immunostaining of NEXMIF and neuronal marker NeuN in brain slices of adult female mice shows a reduction in NEXMIF-expressing neurons in CA1 region of Het hippocampus (D-F, scale bar = 30 µm; E: $t_{(20)} = 7.571$, $p < 0.0001$, F: $t_{(12)} = 1.327$, $p = 0.2092$) and L2/3 of the somatosensory cortex (G-I, scale bar = 50 µm; H: $t_{(27)} = 6.693$, $p < 0.0001$, I: $t_{(18)} = 0.4492$, $p = 0.6587$). n = 10–16 slices, 60–800 cells each. **(J)** Representative mosaic distribution of NEXMIF-expressing (NEXMIF^{+}; yellow) and NEXMIF negative neurons (NEXMIF^{-}; pink) in the somatosensory cortex of WT and *Nexmif* $^{\pm}$ mice. Scale bar = 50 µm. **(K)** Ratios of NEXMIF^{+} and NEXMIF^{-} neurons from the cortex of individual *NEXMIF* $^{\pm}$ mice. *$p < 0.05$, **$p < 0.01$ ***$p < 0.001$, ns = not significant. Error bars represent the SEM. (For interpretation of the references to colour in this figure legend, the reader is referred to the Web version of this article.)

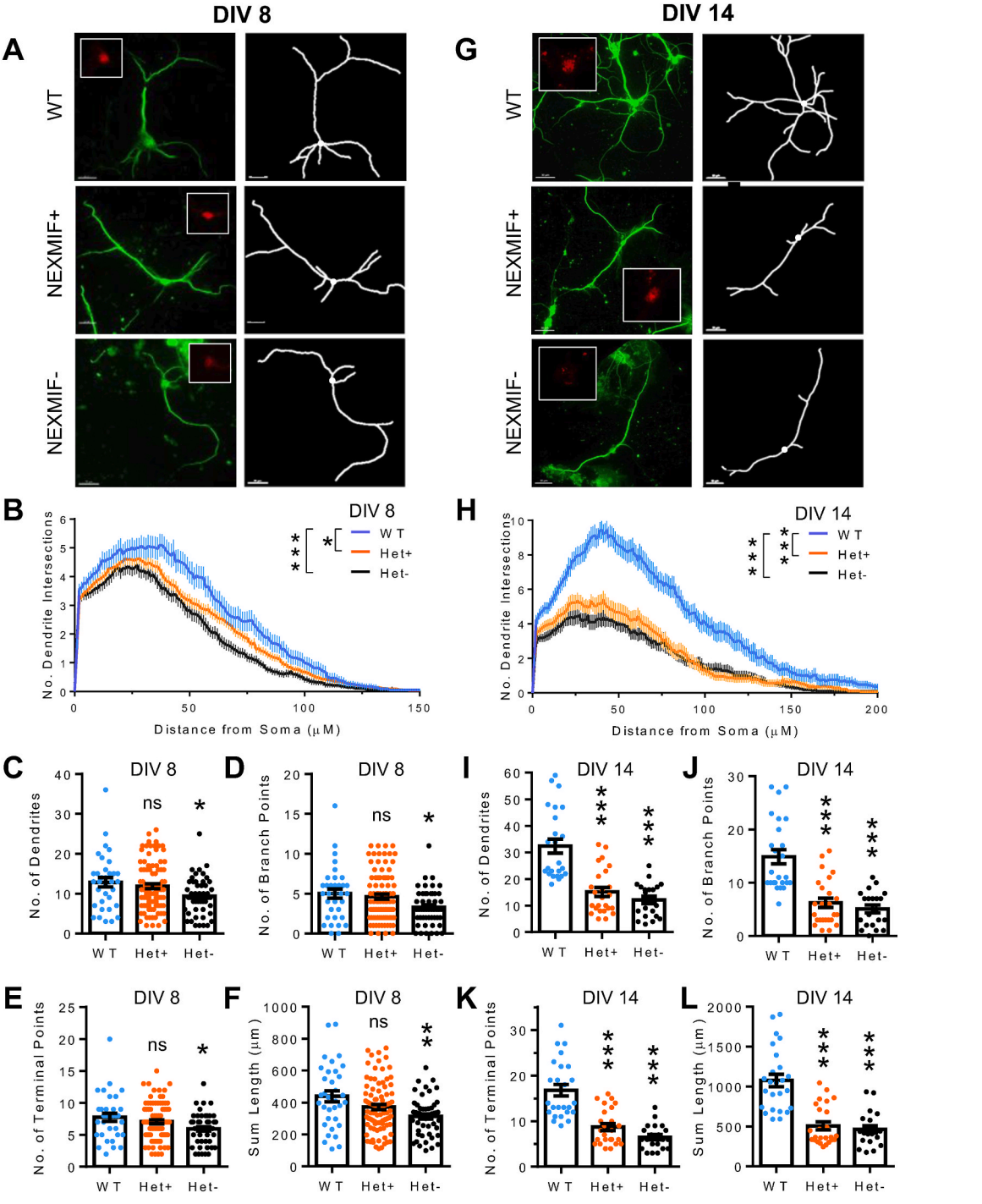

(caption on next page)

Fig. 6. Mosaic loss of NEXMIF results in a decrease in neurite outgrowth in primary neurons **(A)** Representative images (left) and traces (right) of MAP2 immunostained primary cortical neurons from WT or *Nexmif* $^{\pm}$ brains at DIV 8. Inset is immunostaining of NEXMIF, showing a mosaic mixture of NEXMIF^{+} and NEXMIF^{-} neurons. Scale bars = 20 μm. **(B)** Sholl analysis reveals a decrease in dendritic arbor complexity for both NEXMIF^{+} and NEXMIF^{-} neurons at DIV 8 ($F_{(2,172)} = 6.901$, $p = 0.0013$ between genotypes; $F_{(150,\ 25800)} = 2.197$, $p < 0.0001$ between radius). **(C–F)** The number of dendrites (C), branch points (D), terminal points (E), and the sum length of dendrites (F) were decreased in NEXMIF^{-} neurons at DIV 8. **(G)** Representative images and traces of cortical neurons at DIV 14. **(H)** Sholl analysis shows reduced complexity for both NEXMIF^{+} and NEXMIF^{-} neurons at DIV 14 ($F_{(2,68)} = 27.13$, $p < 0.0001$ between genotypes; $F_{(200,\ 13600)} = 137.7$, $p < 0.0001$ between radius). **(I–L)** The number of dendrites (I), branch points (J), terminal points (K), and the sum length of dendrites (L) were decreased in both NEXMIF^{+} and NEXMIF^{-} neurons at DIV 14. (No. of Dendrites: $F_{(2,40)} = 27.98$, $p < 0.0001$ between genotypes; $F_{(1,20)} = 67.95$, $p < 0.0001$ between time points; No. of Branch Points: $F_{(2,40)} = 22.04$, $p < 0.0001$ between genotypes; $F_{(1,20)} = 27.88$, $p < 0.0001$ between time points; No. of Terminal Points: $F_{(2,40)} = 28.42$, $p < 0.0001$ between genotypes; $F_{(1,20)} = 34.27$, $p < 0.0001$ between time points, Sum Length: $F_{(2,40)} = 29.77$, $p < 0.0001$ between genotypes; $F_{(1,20)} = 55.22$, $p < 0.0001$ between time points). n = 30–90 cells/group. Het+, NEXMIF^{+}/NEXMIF-expressing; Het-, NEXMIF^{-}/NEXMIF lacking. *$p < 0.05$, **$p < 0.01$ ***$p < 0.001$, ns = not significant. Error bars represent the SEM.

WT mice, which did spend more time in the target quadrant (Fig. 4I and J). These findings indicate that *NEXMIF* haploinsufficiency causes defects in spatial memory, which may contribute to the cognitive impairments observed in human females.

5.5. Heterozygous Nexmif mice demonstrate mosaic expression of NEXMIF

Due to the random inactivation of either X chromosome, the X-linked gene *Nexmif* is predicted to be expressed in a mosaic manner in heterozygous female mice, leading to either normal expression or complete loss of NEXMIF in individual neurons. This type of mosaic expression has been observed in other haploinsufficient X-linked genes [51–56]. To determine the NEXMIF expression pattern in the brain, we used a NEXMIF specific antibody to immunolabel NEXMIF both *ex vivo* and *in vivo*. First, we generated primary neuronal cultures from *Nexmif* $^{\pm}$ mice or WT littermate controls. These neuron cultures were maintained for 6 days (Days in vitro 6; DIV 6) and were probed for NEXMIF expression. Our previous work indicated that NEXMIF localizes to the nuclei of neurons, but not glia [25]. Consistent with this, NEXMIF was expressed in the nuclei of *Nexmif* $^{\pm}$ neurons as seen by colocalization with the nuclear dye Hoechst (Fig. 5A). Consistent with random XCI, we found that some neurons from *Nexmif* $^{\pm}$ mice expressed NEXMIF while others did not (Fig. 5A). Quantification of the *Nexmif* $^{\pm}$ neurons revealed approximately 70 % of cells expressed NEXMIF (Fig. 5B) to the same level as WT neurons (Fig. 5C), whereas the remaining 30 % of cells were NEXMIF negative.

As the XCI patterning varies between individuals, we quantified the mosaic expression of NEXMIF *in vivo* from adult *Nexmif* $^{\pm}$ mice and WT littermate controls. To do this we used immunohistochemistry to probe for NEXMIF, as well as the neuronal marker NeuN, in brain slices of both the CA1 region of the hippocampus (Fig. 5D) and L2/3 of the somatosensory cortex (Fig. 5G and J). We found mosaic expression of NEXMIF in both hippocampus (Fig. 5E) and somatosensory cortex (Fig. 5H) with NEXMIF expressed respectively in 60 % and 65 % of NeuN positive neurons from *Nexmif* $^{\pm}$ brain slices. Consistent with the in vitro data, the level of NEXMIF expression in these NEXMIF positive neurons was similar to that of neurons from WT mice in both the hippocampus (Fig. 5F) and the somatosensory cortex (Fig. 5I). When the ratio of NEXMIF^{+} vs. NEXMIF^{-} neurons was analyzed in individual animals, we found no cases of skewing (>75:25 ratio) in our haploinsufficient mice (Fig. 5K).

5.6. Mosaic loss of NEXMIF impairs the development of neuronal morphology

One of the key phenotypes observed in neurons lacking NEXMIF is impairments in neurite extension [24,25,57]. We therefore investigated the effect of mosaic loss of NEXMIF on the development of neuronal morphology. To do this, we cultured primary cortical neurons from WT or *Nexmif* $^{\pm}$ brains and immunostained for MAP2 to label the dendrites at DIV 8 (Fig. 6A). Given the mosaic expression of NEXMIF in heterozygote females, we also immunostained for NEXMIF to identify neuron cell types in the *Nexmif* $^{\pm}$ cultures. Consistent with our previous study of *Nexmif* knockdown [25], Sholl analysis revealed a decrease in dendritic arbor complexity for NEXMIF^{-} neurons in the *Nexmif* $^{\pm}$ cultures (Fig. 6B). Further analysis demonstrated that the NEXMIF-lacking (NEXMIF^{-}) neurons had a significant reduction in total number of dendrites, number of branch points, and number of terminal points, as well as a decrease in the total sum length of dendrites (Fig. 6C–F). Similar changes were also detected in NEXMIF^{-} neurons at DIV 14 (Fig. 6G– L). Strikingly, NEXMIF-expressing (NEXMIF^{+}) neurons from the *Nexmif* $^{\pm}$ culture also showed a reduction in dendritic morphology when compared to WT controls (Fig. 6B and 6H-6L). These impairments in dendrite morphology were also observed in primary hippocampal neurons from WT or *Nexmif* $^{\pm}$ animals (Fig. 8).

To further examine the effect of NEXMIF haploinsufficiency on neurite extension, we examined axon outgrowth in primary neuronal cultures from WT or *Nexmif* $^{\pm}$ brains. DIV 3 cortical (Fig. 9A) or hippocampal neurons (Fig. 9D) were immunolabeled for Tau to label axons. Quantification of axonal length and the number of axon branches revealed reduced axonal outgrowth and in both NEXMIF+ and NEXMIF- neurons from the cortex (Fig. 9BandC) and the hippocampus (Fig. 9EandF). Collectively, this data demonstrates that in a mosaic network of mixed cell types, the loss of NEXMIF in some neurons not only causes developmental defects in those neurons themselves, but also *in trans* affects the neighboring neurons which have intact NEXMIF expression.

5.7. Nexmif haploinsufficiency results in reduced spine density

Dysregulation of spine and synapse formation has been recognized as one of the most common cellular defects in ASD. Indeed, a

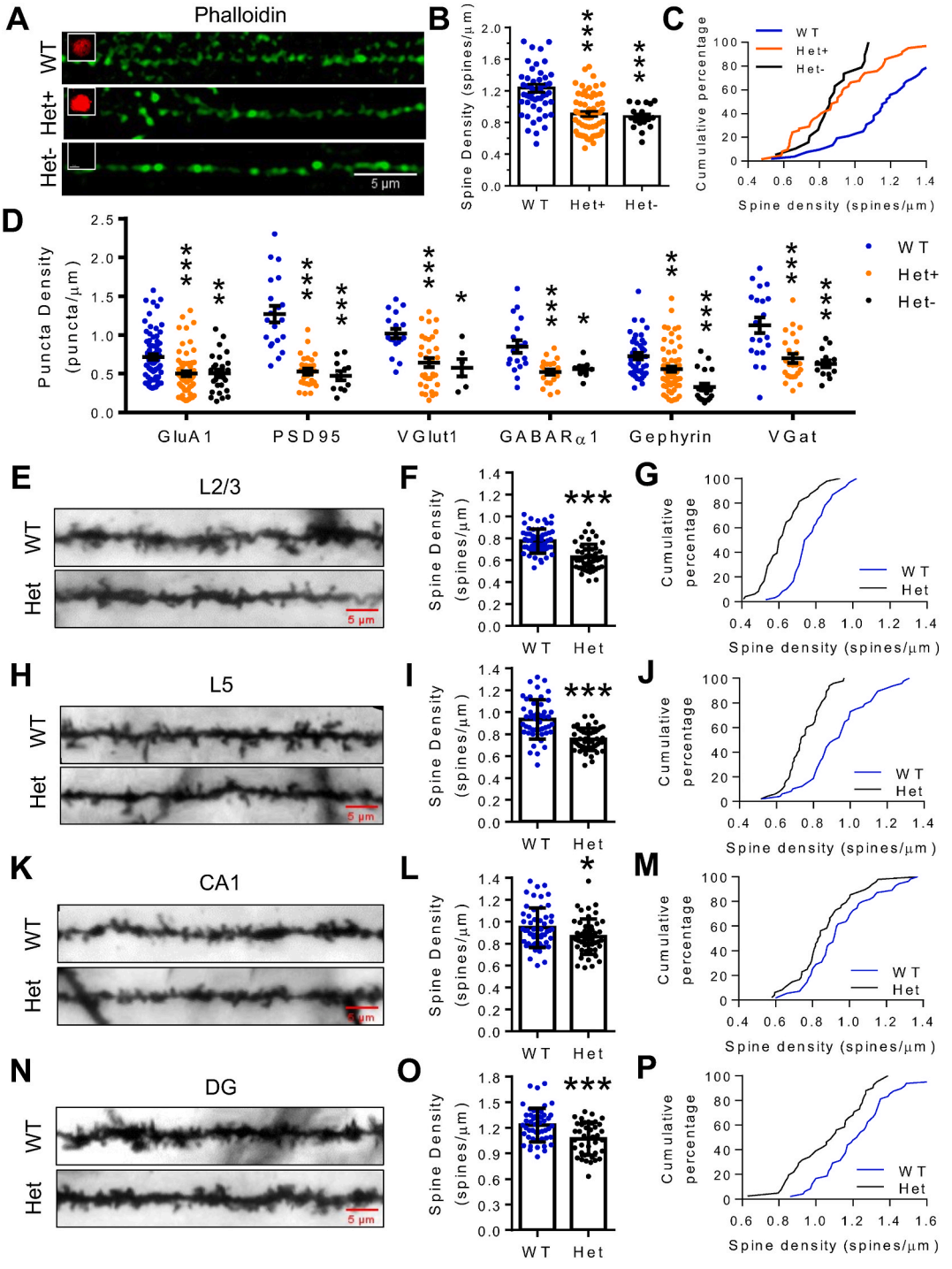

(caption on next page)

Fig. 7. Aberrant dendritic spines and synapses in *Nexmif* Het mice (A) Representative images of DIV 12 primary cortical neurons from WT or *Nexmif* $^{\pm}$ mice immunostained for NEXMIF and labeled for actin with Phalloidin. Inset is immunostaining of NEXMIF, showing a mosaic mixture of NEXMIF^{+} and NEXMIF^{-} neurons. Scale bar = 5 μm. **(B–C)** Spine density was decreased in both NEXMIF^{+} and NEXMIF^{-} neurons. ($F_{(2,130)} = 20.29$, $p < 0.0001$, $n = 19$–60 dendrites/group). **(D)** Quantification of puncta density of synaptic markers. DIV 12 cortical cultures of both NEXMIF^{+} and NEXMIF^{-} neurons were immunostained with antibodies against GluA1 ($F_{(2,171)} = 12.94$, $p < 0.0001$), PSD95 ($F_{(2,56)} = 37.19$, $p < 0.0001$), VGlut1 ($F_{(2,54)} = 9.754$, $p = 0.0002$), GABARα1 ($F_{(2,45)} = 9.887$, $p = 0.0003$), gephyrin ($F_{(2,123)} = 19.17$, $p < 0.0001$), and VGat ($F_{(2,55)} = 12.12$, $p < 0.0001$), respectively. $n = 7$–80 cells/group. **(E–P)** Spines were analyzed from WT or *Nexmif* $^{\pm}$ brain slices following Golgi staining. Spine density was decreased in L2/3 neurons of the somatosensory cortex (E–G) ($t_{(106)} = 6.727$, $p < 0.0001$), L5 neurons of the somatosensory cortex (H–J) ($t_{(94)} = 6.114$, $p < 0.0001$), CA1 neurons of the hippocampus (K–M) ($t_{(101)} = 2.422$, $p = 0.0172$), and the dentate gyrus neurons (N–P) ($t_{(87)} = 3.866$, $p = 0.0002$). Scale bar = 5 μm. $n = 48$–60 dendrites/group. Het+, NEXMIF^{+}/NEXMIF-expressing; Het-, NEXMIF^{-}/NEXMIF lacking. $^{*}p < 0.05$, $^{**}p < 0.01$ $^{***}p < 0.001$. Error bars represent the SEM.

dramatic reduction in spine density was observed in the hippocampi of adult *Nexmif* $^{-/y}$ KO mice [26]. To determine possible changes in spine development in neurons from *Nexmif* $^{\pm}$ mice in vitro, we cultured primary cortical neurons from WT or *Nexmif* $^{\pm}$ brains and applied phalloidin at DIV 12 to label actin-rich spines (Fig. 7A). In line with the *Nexmif* $^{-/y}$ results, we observed a significant decrease in spine density for NEXMIF^{-} neurons compared to neurons from WT brains (Fig. 7B and C). Interestingly, NEXMIF $^{+}$ neurons in the *Nexmif* $^{\pm}$ culture showed a decrease in spine density similar to that of the NEXMIF^{-} neurons. By immunocytochemistry, we then examined the expression and localization of major synaptic proteins including GluA1, PSD95, VGlut1, GABARa 1, Gephyrin, and VGat. We found that puncta density of each of these synaptic proteins was significantly reduced in both NEXMIF^{+} and NEXMIF^{-} neurons from the *Nexmif* $^{\pm}$ culture, as compared to neurons from the WT culture (Fig. 7D; Supplementary Figs. 7–1).

In order to observe changes in spine density *in vivo*, we performed Golgi staining on brains of adult WT and *Nexmif* $^{\pm}$ mice. Because Golgi staining randomly labels neurons, the specific cell type regarding NEXMIF expression could not be determined. Therefore, the Golgi stained neurons were combined for structural analysis. Compared to WT controls, a significant decrease in spine density was detected in neurons from *Nexmif* $^{\pm}$ brains (Fig. 7E– P). This change was apparent in all brain regions measured, including L2/3 (Fig. 7E–G) and L5 (Fig. 7H–J) from the somatosensory cortex and CA1 (Fig. 7K–M) and the dentate gyrus (Fig. 7N– P) from the hippocampus. Closer examination of this data revealed that the neurons from *Nexmif* $^{\pm}$ brains did not fall into two distinct groups as predicted to result from the two subsets of NEXMIF^{+} and NEXMIF^{-} neurons, suggesting that the NEXMIF^{+} cells were likely also affected, as we found in cultured neurons (Fig. 7A–C).

Discussion

In this study, we successfully established and characterized a haploinsufficient *Nexmif* $^{\pm}$ mouse line, and we find that the haploinsufficient female mice display ASD-like behavioral phenotypes. As compared to wild-type female controls, *Nexmif* $^{\pm}$ female mice demonstrated reduced sociability and preference for social novelty, behaviors which have been associated with the hippocampus and the anterior region of the insular cortex [58,59]. The *Nexmif* $^{\pm}$ female mice also showed significant changes in marble burying, grooming, and rearing behaviors, which are associated with the neocortex and hippocampus, respectively [60,61]. We also found that the *Nexmif* $^{\pm}$ females displayed increased activity in an open field and significant impairments in hippocampal-dependent spatial memory, as measured by the Barnes Maze. In line with findings of milder communication phenotypes in females with NEXMIF-dependent ASD [16,17], *Nexmif* $^{\pm}$ female mice showed moderate changes in ultrasonic vocalizations in isolated pups. Thus, our findings validify this transgenic line as a model for NEXMIF-dependent ASD in females.

We also investigated cellular and molecular phenotypes in the brains of *Nexmif* $^{\pm}$ mice. We found the heterozygous brains demonstrate a mosaic mixture of wild-type and null mutant neurons caused by random X-inactivation in both the hippocampus and the somatosensory cortex. In primary neuronal cultures of the brains of the transgenic females, we found that both NEXMIF^{+} and NEXMIF^{-} neurons demonstrated aberrant dendritic arborization and reductions in spine and synapse density. Both groups of neurons also showed reductions in the puncta density of key synaptic proteins including GluA1, PSD95, VGlut1 at excitatory synapses, and GABARα1, Gephyrin, and VGat at inhibitory synapses. Thus, the loss of NEXMIF affects not only the mutant cells themselves, but also the neighboring NEXMIF^{+} cells. These surprising findings indicate a non-cell autonomous effect from loss of NEXMIF. It is possible that *NEXMIF* haploinsufficiency causes a reduction of secretory molecules in the extracellular milieu, leading to developmental defects in all cells.

Studies of humans with *NEXMIF*-dependent ASD have demonstrated a significant difference in disease phenotypes between hemizygous knockout males and heterozygous females. Males tend to have more severe impairments in language (58 % nonverbal) and cognition (74 % severe to profound ID) than females (10 % nonverbal; 32 % severe to profound ID) [17]. Consistently, our previous work on the *Nexmif* $^{-/y}$ male mouse model shows that the KO males have significant impairments in communication [26], while the current study shows only moderate changes in communication for haploinsufficient *Nexmif* $^{\pm}$ females. In haploinsufficient females, variations in phenotypic severity could result from skewed XCI [62–69]. Of the 32 females with *Nexmif* variants who have been tested for XCI skewing, 25 showed random (<75:25) XCI patterning without skewing. Additionally, when comparing sisters within patient families, no correlation was found between extent of XCI skewing and disease phenotype, indicating skewing itself is unlikely to be responsible for phenotypic variations [17]. Although these findings were from peripheral blood cells, they are in agreement with our findings in the female mouse model, which shows no signs of significant skewing in NEXMIF expression in the brains of heterozygous female mice.

In the brain, mosaic expression of NEXMIF could lead to structural and functional abnormalities via multiple potential mechanisms.

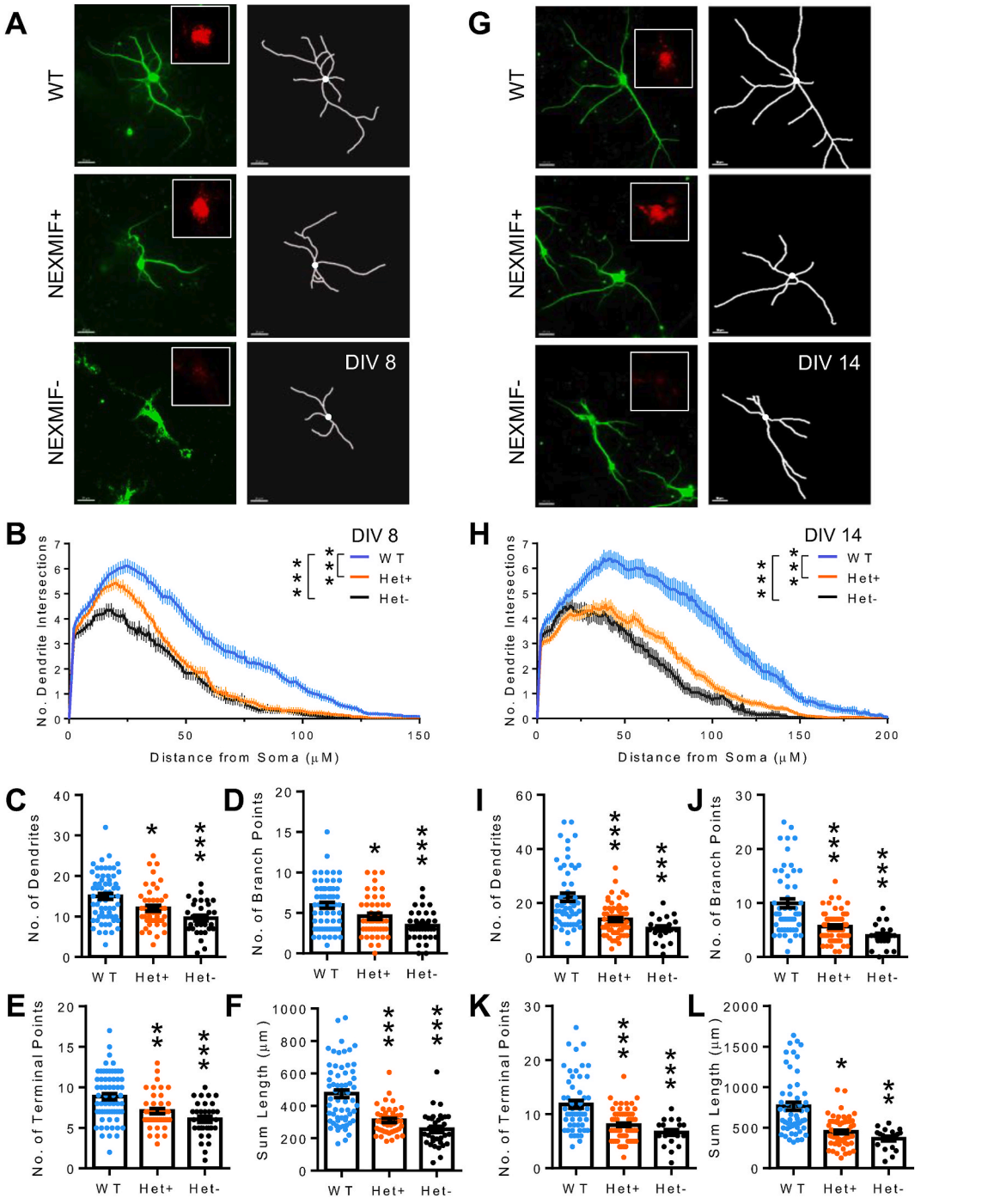

(caption on next page)

Fig. 8. Hippocampal neurons of Nexmif heterozygous mice show abnormal dendritic arborization (A) Representative images (left) and traces (right) of MAP2 immunostained primary hippocampal neurons from WT or *Nexmif* $^{\pm}$ brains at DIV 8. Inset is immunostaining of NEXMIF, showing a mosaic mixture of NEXMIF^{+} and NEXMIF^{-} neurons. Scale bars = 20 μm. **(B)** Sholl analysis reveals a decrease in dendritic arbor complexity for both NEXMIF^{+} and NEXMIF^{-} neurons at DIV 8 ($F_{(2,141)} = 29.35$, $p < 0.0001$ between genotypes; $F_{(150,\ 21150)} = 350.5$, $p < 0.0001$ between radius). **(C–F)** The number of dendrites (C), branch points (D), terminal points (E), and sum length of dendrites (F) were decreased in both groups of *Nexmif* $^{\pm}$ neurons at DIV 8. **(G)** Representative images and traces of hippocampal neurons at DIV 14. **(H)** Sholl analysis shows reduced complexity for both NEXMIF^{+} and NEXMIF^{-} neurons at DIV 14 ($F_{(2,68)} = 27.13$, $p < 0.0001$ between genotypes; $F_{(200,\ 13600)} = 137.7$, $p < 0.0001$ between radius). **(I–L)** The number of dendrites (I), branch points (J), terminal points (K), and the sum length of dendrites (L) were decreased in both NEXMIF^{+} and NEXMIF^{-} neurons at DIV 14. (No. of Dendrites: $F_{(2,38)} = 46.72$, $p < 0.0001$ between genotypes; $F_{(1,19)} = 25.77$, $p < 0.0001$ between time points; No. of Branch Points: $F_{(2,38)} = 31.15$, $p < 0.0001$ between genotypes; $F_{(1,19)} = 20.49$, $p = 0.0002$ between time points; No. of Terminal Points: $F_{(2,38)} = 50.81$, $p < 0.0001$ between genotypes; $F_{(1,19)} = 39.64$, $p < 0.0001$ between time points, Sum Length: $F_{(2,38)} = 40.62$, $p < 0.0001$ between genotypes; $F_{(1,19)} = 32.38$, $p < 0.0001$ between time points). $n = 20$–70 cells/group. Het+, NEXMIF^{+}/NEXMIF-expressing; Het-, NEXMIF^{-}/NEXMIF lacking. $*p < 0.05$, $**p < 0.01$ $***p < 0.001$. Error bars represent the SEM.

While the most direct causal factor is the loss of *NEXMIF* in the NEXMIF^{-} neurons, the unbalanced NEXMIF expression among mosaic neurons in the brain can lead to further disruptions. To compensate for the overall reduction of NEXMIF in the brain, NEXMIF expression may be upregulated in NEXMIF^{+} cells. This global compensation would result in overexpression and a hyper-dosage of the protein in the NEXMIF $^{+}$ neurons. Our findings indicate that this scenario did not occur in the *Nexmif* haploinsufficient females. Second, if the effect of loss of *NEXMIF* is mediated, at least partially, via secretory signaling molecules, changes in NEXMIF expression could affect all neurons in the brain. In fact, we found comparable defects in dendritic structure and spine formation in both NEXMIF^{+} and NEXMIF^{-} neurons. Interestingly, the impaired dendritic arborization phenotype became more severe in NEXMIF^{+} cortical neurons at DIV 14 than at DIV 8. It is possible that, at the early stage, a lack of NEXMIF only affects NEXMIF^{-} neurons, and at a later phase, the NEXMIF^{+} neurons are affected from neighboring NEXMIF^{-} neurons, probably due to changes in extracellular cues. Indeed, altered expression of several ASD genes has been associated with impaired dendritic growth and spine morphology. In the cortical neurons of *Ube3a* 2X ASD mice, we previously found that increased *Ube3a* gene dosage results in reduced dendritic branching and spine density due to over-pruning of dendrites [70]. Moreover, maternal loss of *Ube3a*, which is associated with the development of Angelman syndrome, also reduced dendritic spine density in the mouse visual cortex due to increased spine elimination [71]. Loss of the Rett syndrome gene *Mecp2* induced reductions in pyramidal dendritic arbor complexity and spine density, while overexpression of MeCP2 protein increased layer 5 pyramidal neuron spine density and dendritic overgrowth in mice [72]. Interestingly, loss of the Fragile X syndrome gene *Fmr1* is not only associated with unusually long dendritic spines in human patients and in *Fmr1* knockout rodent models, but was also found to have a transient effect on spine and dendritic outgrowth depending on the developmental timepoint [73]. These studies highlight the importance of ASD gene dosage in proper neuronal morphogenesis.

Given the mutual innervation between NEXMIF^{+} and NEXMIF^{-} neurons, the *trans* effects on NEXMIF $^{+}$ neurons could also result from aberrant interneuronal communication. Not only might this account for the phenotypes in the NEXMIF $^{+}$ neurons, but the cell-cell interactions between wild type and mutant neurons in the brain of heterozygotes could also disrupt the overall neuronal circuitry in a way that is different, and possibly more severe, than from the complete loss of *Nexmif* in KOs. Such a "cellular interference" or "metabolic interference" mechanism [74] has been observed in other heterozygous X-linked diseases such as *ARHGEF9*-dependent ASD [75], *PCDH19*-linked epilepsy and mental retardation [76], craniofrontonasal syndrome [77,78], and sporadic infantile epileptic encephalopathy [76,79].

While a number of somatic gene mutations are known to lead to ASD in heterozygous females [45,80–84], only a few X-linked genes, including *NEXMIF*, have been reported to be implicated in ASD by haploinsufficiency. For X-linked genes, heterozygous females generally have a milder disease phenotype, or are unaffected carriers, due to sufficient gene expression from the normal allele, which is not possible in the male counterparts. However, there are some cases of manifesting heterozygotes, in which heterozygous expression of an X-linked gene results in a more severe phenotype [46,65,67], such as in the heterozygous X-linked neurological disorders Rett syndrome [66], fragile X syndrome [85,86], *CASK*-associated mental retardation [87,88], and loss of *PCDH19* [56,89]. In some cases, the disease phenotype results from XCI skewing which leads to biased silencing of the X chromosome containing the normal allele, but this seems not to be the case for individuals with *NEXMIF* mutations. A number of computational studies have attempted to identify genes which cannot tolerate the loss of one of the two alleles [90–94]. It has been shown that haploinsufficient genes are enriched in several gene ontology categories including transcription factors and phenotypes including neurodevelopmental disorders [90]. Notably, *NEXMIF* is predicted to be a haploinsufficient gene [94], and although its direct role remains unknown, its nuclear localization suggests it may play a role in gene expression.

In summary, our results show that the *Nexmif* $^{\pm}$ animals demonstrate ASD-like behaviors, making it a useful model for further study of *Nexmif* and ASD. NEXMIF is expressed in a mosaic pattern in the brains of these animals. Therefore, the heterozygous female mice provide a unique neural network intertwined by mutual innervation between and among the NEXMIF^{+} and NEXMIF^{-} neurons in the

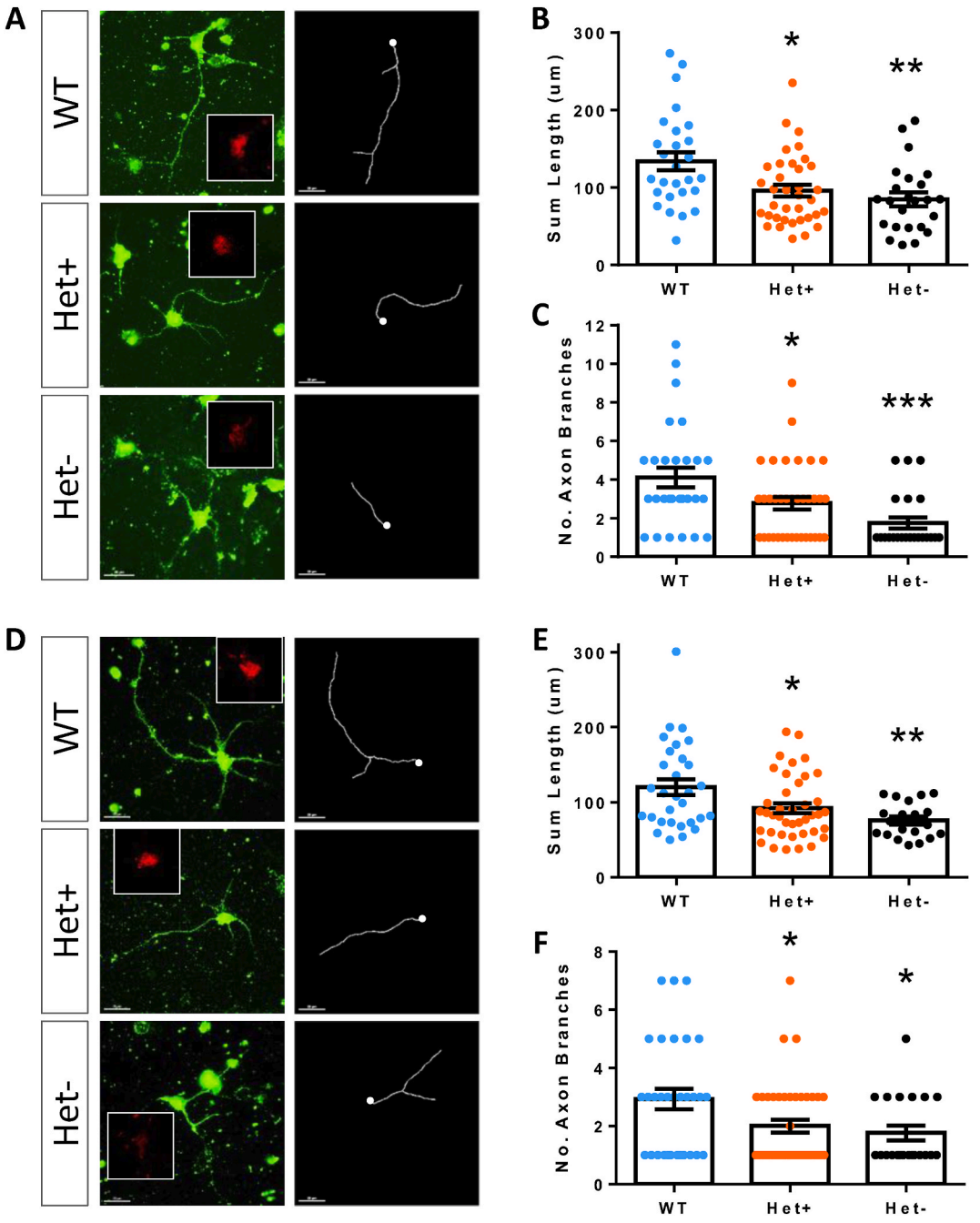

Fig. 9. NEXMIF haploinsufficiency leads to impaired axonal outgrowth (A) Representative images of Tau immunostained primary cortical neurons from WT or Nexmif±brains at DIV 3. (B, C) The sum length of axons (B) ($F(2,84) = 7.020$, $p = 0.0015$) and the number of axon branches (C) ($F(2,85) = 8.182$, $p = 0.0006$) were decreased in only NEXMIF- cortical neurons. n = 24–36 cells. (D) Representative images of Tau immunostained primary hippocampal neurons from WT or Nexmif±brains at DIV 3. (E, F) The sum length of axons (E) ($F(2,87) = 6.495$, $p = 0.0023$) and the number of axon branches (F) ($F(2,90) = 4.451$, $p = 0.0143$) were decreased in both NEXMIF- and NEXMIF + hippocampal neurons. n = 21–41 cells. Error bars represent the SEM.

brain. Additionally, the heterozygous female model is of particular interest for future study for its potential to rescue the loss of *Nexmif* from the endogenous normal *Nexmif* allele by specific reactivation of the wild type allele on the silenced X chromosome, as shown to be a promising strategy in *MECP2*-linked Rett syndrome [95]. The *Nexmif* $^{\pm}$ line will therefore be of great value for further study of the mechanisms underlying *NEXMIF*-dependent ASD, as well as the development of effective therapeutic approaches.

Data availability statement

Data included in article/supplementary material/referenced in article.

CRediT authorship contribution statement

Margaret O'Connor: Data curation, Formal analysis, Investigation, Methodology, Validation, Visualization, Writing – original draft, Conceptualization. **Hui Qiao:** Formal analysis, Validation, Visualization, Investigation. **KathrynAnn Odamah:** Validation, Visualization, Writing – review & editing, Investigation. **Pedro Casariego Cerdeira:** Formal analysis, Investigation, Visualization. **Heng-Ye Man:** Conceptualization, Data curation, Funding acquisition, Investigation, Methodology, Project administration, Supervision, Validation, Visualization, Writing – review & editing, Writing – original draft.

Declaration of competing interest

The authors declare that they have no known competing financial interests or personal relationships that could have appeared to influence the work reported in this paper.

Acknowledgements

We would like to thank the members of the Man Lab for supportive discussion. This work was supported by NIH grants R01 MH079407, R21 MH133014 and the Harvard/MIT Joint Research Grants Program in Basic Neuroscience. The authors declare no competing financial interests.

Appendix A. Supplementary data

Supplementary data to this article can be found online at https://doi.org/10.1016/j.heliyon.2024.e24703.

References

[1] R.J. Landa, Diagnosis of autism spectrum disorders in the first 3 years of life, Nat. Clin. Pract. Neurol. 4 (2008) 138–147, https://doi.org/10.1038/ncpneuro0731.
[2] G. Huguet, E. Ey, T. Bourgeron, The genetic Landscapes of autism spectrum disorders, Annu. Rev. Genom. Hum. Genet. 14 (2013) 191–213, https://doi.org/10.1146/annurev-genom-091212-153431.
[3] B.A. Fernandez, S.W. Scherer, Syndromic autism spectrum disorders: moving from a clinically defined to a molecularly defined approach, Dialogues Clin. Neurosci. 19 (2017) 353–371, https://doi.org/10.31887/DCNS.2017.19.4/sscherer.
[4] S. Banerjee-Basu, A. Packer, SFARI Gene: an evolving database for the autism research community, DMM Dis Model Mech 3 (2010) 133–135, https://doi.org/10.1242/dmm.005439.
[5] B.S. Abrahams, D.E. Arking, D.B. Campbell, H.C. Mefford, E.M. Morrow, L.A. Weiss, I. Menashe, T. Wadkins, S. Banerjee-Basu, A. Packer, SFARI Gene 2.0: a community-driven knowledgebase for the autism spectrum disorders (ASDs), Mol. Autism. 4 (2013) 36, https://doi.org/10.1186/2040-2392-4-36.
[6] F. Happé, A. Ronald, R. Plomin, Time to give up on a single explanation for autism, Nat. Neurosci. 9 (2006) 1218–1220, https://doi.org/10.1038/nn1770.
[7] B.S. Abrahams, D.H. Geschwind, Advances in autism genetics: on the threshold of a new neurobiology, Nat. Rev. Genet. 9 (2008) 341–355, https://doi.org/10.1038/nrg2346.
[8] H. Yoo, Genetics of autism spectrum disorder: current status and possible clinical applications, Exp Neurobiol 24 (2015) 257–272, https://doi.org/10.5607/en.2015.24.4.257.
[9] L. Rylaarsdam, A. Guemez-Gamboa, Genetic causes and modifiers of autism spectrum disorder, Front. Cell. Neurosci. 13 (2019), https://doi.org/10.3389/fncel.2019.00385.
[10] V. Cantagrel, A.-M. Lossi, S. Boulanger, D. Depetris, M.-G. Mattei, J. Gecz, C.E. Schwartz, L. Van Maldergem, L. Villard, Disruption of a new X linked gene highly expressed in brain in a family with two mentally retarded males, J. Med. Genet. 41 (2004) 736–742, https://doi.org/10.1136/jmg.2004.021626.
[11] A. Charzewska, S. Rzońca, M. Janeczko, M. Nawara, M. Smyk, J. Bal, D. Hoffman-Zacharska, A duplication of the whole *KIAA2022* gene validates the gene role in the pathogenesis of intellectual disability and autism, Clin. Genet. 88 (2015) 297–299, https://doi.org/10.1111/cge.12528.
[12] Y. Kuroda, I. Ohashi, T. Naruto, K. Ida, Y. Enomoto, T. Saito, J. Nagai, T. Wada, K. Kurosawa, Delineation of the KIAA2022 mutation phenotype: two patients with X-linked intellectual disability and distinctive features, Am J Med Genet Part A 167 (2015) 1349–1353, https://doi.org/10.1002/ajmg.a.37002.
[13] N. Lambert, C. Dauve, E. Ranza, P. Makrythanasis, F. Santoni, F. Sloan-Béna, S. Gimelli, J.-L. Blouin, M. Guipponi, A. Bottani, S.E. Antonarakis, M.M. Kosel, J. Fluss, A. Paoloni-Giacobino, Novel NEXMIF pathogenic variant in a boy with severe autistic features, intellectual disability, and epilepsy, and his mildly affected mother, J. Hum. Genet. 63 (2018) 847–850, https://doi.org/10.1038/s10038-018-0459-2.
[14] M. Lorenzo, I. Stolte-Dijkstra, P. van Rheenen, R.G. Smith, T. Scheers, J.S. Walia, Clinical spectrum of *KIAA2022* pathogenic variants in males: case report of two boys with *KIAA2022* pathogenic variants and review of the literature, Am J Med Genet Part A 176 (2018) 1455–1462, https://doi.org/10.1002/ajmg.a.38667.
[15] T. Alarcon-Martinez, A. Khan, K.A. Myers, Torpedo maculopathy associated with NEXMIF mutation, Mol. Syndromol. (2019), https://doi.org/10.1159/000498835.
[16] P.K. Panda, I.K. Sharawat, K. Joshi, L. Dawman, R. Bolia, Clinical spectrum of KIAA2022/NEXMIF pathogenic variants in males and females: report of three patients from Indian kindred with a review of published patients, Brain Dev. 42 (2020) 646–654, https://doi.org/10.1016/j.braindev.2020.06.005.

[17] H. Stamberger, et al., NEXMIF encephalopathy: an X-linked disorder with male and female phenotypic patterns, Genet. Med. 2 (2021) 363–373, https://doi.org/10.1038/s41436-020-00988-9.
[18] E. Athanasakis, D. Licastro, F. Faletra, A. Fabretto, S. Dipresa, D. Vozzi, A. Morgan, A.P. d'Adamo, V. Pecile, X. Biarnés, P. Gasparini, Next generation sequencing in nonsyndromic intellectual disability: from a negative molecular karyotype to a possible causative mutation detection, Am J Med Genet Part A 164 (2014) 170–176, https://doi.org/10.1002/ajmg.a.36274.
[19] M. Moysés-Oliveira, R.S. Guilherme, V.A. Meloni, A. Di Battista, C.B. de Mello, S. Bragagnolo, D. Moretti-Ferreira, N. Kosyakova, T. Liehr, G.M. Carvalheira, M. I. Melaragno, X-linked intellectual disability related genes disrupted by balanced X-autosome translocations, Am. J. Med. Genet. Part B Neuropsychiatr Genet 168 (2015) 669–677, https://doi.org/10.1002/ajmg.b.32355.
[20] I.M. de Lange, et al., De novo mutations of KIAA2022 in females cause intellectual disability and intractable epilepsy, J. Med. Genet. 53 (2016) 850–858, https://doi.org/10.1136/jmedgenet-2016-103909.
[21] L.S. Farach, H. Northrup, KIAA2022 nonsense mutation in a symptomatic female, Am J Med Genet Part A 170 (2016) 703–706, https://doi.org/10.1002/ajmg.a.37479.
[22] R. Webster, M.T. Cho, K. Retterer, F. Millan, C. Nowak, J. Douglas, A. Ahmad, G.V. Raymond, M.R. Johnson, A. Pujol, A. Begtrup, D. McKnight, O. Devinsky, W. K. Chung, De novo loss of function mutations in KIAA2022 are associated with epilepsy and neurodevelopmental delay in females, Clin. Genet. 91 (2017) 756–763, https://doi.org/10.1111/cge.12854.
[23] D. Wu, C. Ji, Z. Chen, K. Wang, Novel NEXMIF gene pathogenic variant in a female patient with refractory epilepsy and intellectual disability, Am J Med Genet Part A 182 (2020) 2765–2772, https://doi.org/10.1002/ajmg.a.61848.
[24] L. Van Maldergem, Q. Hou, V.M. Kalscheuer, M. Rio, M. Doco-Fenzy, A. Medeira, A.P.M. de Brouwer, C. Cabrol, S.A. Haas, P. Cacciagli, S. Moutton, E. Landais, J. Motte, L. Colleaux, C. Bonnet, L. Villard, J. Dupont, H.-Y. Man, Loss of function of KIAA2022 causes mild to severe intellectual disability with an autism spectrum disorder and impairs neurite outgrowth, Hum. Mol. Genet. 22 (2013) 3306–3314, https://doi.org/10.1093/hmg/ddt187.
[25] J. Gilbert, H.-Y. Man, The X-linked autism protein KIAA2022/KIDLIA regulates neurite outgrowth via N-cadherin and d-catenin signaling, eNeuro 3 (2016), https://doi.org/10.1523/ENEURO.0238-16.2016. ENEURO.0238-16.2016.
[26] J. Gilbert, M. O'Connor, S. Templet, M. Moghaddam, A. Sinclair, L.-Q. Zhu, W. Xu, H.-Y. Man, NEXMIF/KIDLIA knock-out mouse demonstrates autism-like behaviors, memory deficits, and impairments in synapse formation and function, J. Neurosci. 40 (2020) 237–254, https://doi.org/10.1523/JNEUROSCI.0222-19.2019.
[27] T. Ishikawa, S. Miyata, Y. Koyama, K. Yoshikawa, T. Hattori, N. Kumamoto, K. Shingaki, T. Katayama, M. Tohyama, Transient expression of Xpn, an XLMR protein related to neurite extension, during brain development and participation in neurite outgrowth, Neuroscience 214 (2012) 181–191, https://doi.org/10.1016/j.neuroscience.2012.04.030.
[28] C. Stekelenburg, J.L. Blouin, F. Santoni, N. Zaghloul, E.A. O'Hare, R. Dusaulcy, P. Maechler, V.M. Schwitzgebel, Loss of Nexmif results in the expression of phenotypic variability and loss of genomic integrity, Sci. Rep. 12 (1) (2022) 13815, https://doi.org/10.1038/s41598-022-17845-1.
[29] S.J. Elsässer, K.M. Noh, N. Diaz, C.D. Allis, L.A. Banaszynski, Histone H3.3 is required for endogenous retroviral element silencing in embryonic stem cells, Nature 522 (7555) (2015) 240–244, https://doi.org/10.1038/nature14345.
[30] M. Moysés-Oliveira, A. Di-Battista, M. Zamariolli, V.A. Meloni, S. Bragagnolo, D.M. Christofolini, C.E. Steiner, N. Kosyakova, T. Liehr, A. Reymond, M. I. Melaragno, Breakpoint mapping at nucleotide resolution in X-autosome balanced translocations associated with clinical phenotypes, Eur. J. Hum. Genet. 27 (5) (2019) 760–771, https://doi.org/10.1038/s41431-019-0341-5.
[31] F. Romero-Ferrero, M.G. Bergomi, R. Hinz, F.J.H. Heras, G.G. De Polavieja, idtracker.ai: Tracking all individuals in large collectives of unmarked animals (2018), https://doi.org/10.1038/s41592-018-0295-5.
[32] J.L. Silverman, M. Yang, C. Lord, J.N. Crawley, Behavioral phenotyping assays for mouse models of autism, Nat. Rev. Neurosci. 11 (2010) 490–502, https://doi.org/10.1038/nrn2851.
[33] N. Egashira, A. Tanoue, T. Matsuda, E. Koushi, S. Harada, Y. Takano, G. Tsujimoto, K. Mishima, K. Iwasaki, M. Fujiwara, Impaired social interaction and reduced anxiety-related behavior in vasopressin V1a receptor knockout mice, Behav. Brain Res. 178 (2007) 123–127, https://doi.org/10.1016/j.bbr.2006.12.009.
[34] E. Hashemi, P. Sahbaie, M.F. Davies, J.D. Clark, T.M. DeLorey, Gabrb3 gene deficient mice exhibit increased risk assessment behavior, hypotonia and expansion of the plexus of locus coeruleus dendrites, Brain Res. 1129 (2007) 191–199, https://doi.org/10.1016/j.brainres.2006.10.050.
[35] M.C.M. Balemans, M.M.H. Huibers, N.W.D. Eikelenboom, A.J. Kuipers, R.C.J. van Summeren, M.M.C.A. Pijpers, M. Tachibana, Y. Shinkai, H. van Bokhoven, C. E.E.M. Van der Zee, Reduced exploration, increased anxiety, and altered social behavior: autistic-like features of euchromatin histone methyltransferase 1 heterozygous knockout mice, Behav. Brain Res. 208 (2010) 47–55, https://doi.org/10.1016/j.bbr.2009.11.008.
[36] M. Feyder, et al., Association of mouse Dlg4 (PSD-95) gene deletion and human DLG4 gene variation with phenotypes relevant to autism spectrum disorders and Williams' syndrome, Am J Psychiatry 167 (2010) 1508–1517, https://doi.org/10.1176/appi.ajp.2010.10040484.
[37] M. Kouser, H.E. Speed, C.M. Dewey, J.M. Reimers, A.J. Widman, N. Gupta, S. Liu, T.C. Jaramillo, M. Bangash, B. Xiao, P.F. Worley, C.M. Powell, Loss of predominant shank 3 isoforms results in hippocampus-dependent impairments in behavior and synaptic transmission, J. Neurosci. 33 (2013) 18448–18468, https://doi.org/10.1523/JNEUROSCI.3017-13.2013.
[38] B. Greco, F. Managò, V. Tucci, H.-T. Kao, F. Valtorta, F. Benfenati, Autism-related behavioral abnormalities in synapsin knockout mice, Behav. Brain Res. 251 (2013) 65–74, https://doi.org/10.1016/j.bbr.2012.12.015.
[39] J.N. Lugo, G.D. Smith, E.P. Arbuckle, J. White, A.J. Holley, C.M. Floruta, N. Ahmed, M.C. Gomez, O. Okonkwo, Deletion of PTEN produces autism-like behavioral deficits and alterations in synaptic proteins, Front. Mol. Neurosci. 7 (2014) 27, https://doi.org/10.3389/fnmol.2014.00027.
[40] S.S. Moy, N.V. Riddick, V.D. Nikolova, B.L. Teng, K.L. Agster, R.J. Nonneman, N.B. Young, L.K. Baker, J.J. Nadler, J.W. Bodfish, Repetitive behavior profile and supersensitivity to amphetamine in the C58/J mouse model of autism, Behav. Brain Res. 259 (2014) 200–214, https://doi.org/10.1016/j.bbr.2013.10.052.
[41] A.Ö. Sungur, K.J. Vörckel, R.K.W. Schwarting, M. Wöhr, Repetitive behaviors in the Shank 1 knockout mouse model for autism spectrum disorder: developmental aspects and effects of social context, J. Neurosci. Methods 234 (2014) 92–100, https://doi.org/10.1016/j.jneumeth.2014.05.003.
[42] R. Wurzman, P.A. Forcelli, C.J. Griffey, L.F. Kromer, Repetitive grooming and sensorimotor abnormalities in an ephrin-A knockout model for Autism Spectrum Disorders, Behav. Brain Res. 278 (2015) 115–128, https://doi.org/10.1016/j.bbr.2014.09.012.
[43] M. Bidinosti, et al., CLK2 inhibition ameliorates autistic features associated with SHANK3 deficiency, Science 351 (6278) (2016) 1199–1203, https://doi.org/10.1126/science.aad5487.
[44] C. Delépine, H. Meziane, J. Nectoux, M. Opitz, A.B. Smith, C. Ballatore, Y. Saillour, A. Bennaceur-Griscelli, Q. Chang, E.C. Williams, M. Dahan, A. Duboin, P. Billuart, Y. Herault, T. Bienvenu, Altered microtubule dynamics and vesicular transport in mouse and human MeCP2-deficient astrocytes, Hum. Mol. Genet. 25 (2016) 146–157, https://doi.org/10.1093/hmg/ddv464.
[45] T.C. Jaramillo, H.E. Speed, Z. Xuan, J.M. Reimers, C.O. Escamilla, T.P. Weaver, S. Liu, I. Filonova, C.M. Powell, Novel Shank3 mutant exhibits behaviors with face validity for autism and altered striatal and hippocampal function, Autism Res. 10 (2017) 42–65, https://doi.org/10.1002/aur.1664.
[46] C. Fuchs, L. Gennaccaro, S. Trazzi, S. Bastianini, S. Bettini, V Lo Martire, E. Ren, G. Medici, G. Zoccoli, R. Rimondini, E. Ciani, Heterozygous CDKL5 knockout female mice are a valuable animal model for CDKL5 disorder, Neural Plast. (2018), https://doi.org/10.1155/2018/9726950, 2018.
[47] J. Arranz, E. Balducci, K. Arató, G. Sánchez-Elexpuru, S. Najas, A. Parras, E. Rebollo, I. Pijuan, I. Erb, G. Verde, I. Sahun, M.J. Barallobre, J.J. Lucas, M. P. Sánchez, S. de la Luna, M.L. Arbonés, Impaired development of neocortical circuits contributes to the neurological alterations in DYRK1A haploinsufficiency syndrome, Neurobiol. Dis. 127 (2019) 210–222, https://doi.org/10.1016/j.nbd.2019.02.022.
[48] A.V. Kalueff, A.M. Stewart, C. Song, K.C. Berridge, A.M. Graybiel, J.C. Fentress, Neurobiology of rodent self-grooming and its value for translational neuroscience, Nat. Rev. Neurosci. 17 (2016) 45–59, https://doi.org/10.1038/nrn.2015.8.
[49] O. Sturman, P.L. Germain, J. Bohacek, Exploratory rearing: a context- and stress-sensitive behavior recorded in the open-field test, Stress 21 (2018) 443–452, https://doi.org/10.1080/10253890.2018.1438405.
[50] American Psychiatric Association, Diagnostic and Statistical Manual of Mental Disorders, fifth ed., American Psychiatric Association, 2013.

[51] S.S. Tan, B. Faulkner-Jones, S.J. Breen, M. Walsh, J.F. Bertram, B.E. Reese, Cell dispersion patterns in different cortical regions studied with an X-inactivated transgenic marker, Development 121 (1995) 1029–1039, https://doi.org/10.1242/dev.121.4.1029.

[52] A. Compagni, M. Logan, R. Klein, R.H. Adams, Control of skeletal patterning by EphrinB1-EphB interactions, Dev. Cell 5 (2003) 217–230, https://doi.org/10.1016/s1534-5807(03)00198-9.

[53] R.D. Smrt, R.L. Pfeiffer, X. Zhao, Age-dependent expression of MeCP2 in a heterozygous mosaic mouse model, Hum. Mol. Genet. 20 (2011) 1834–1843, https://doi.org/10.1093/hmg/ddr066.

[54] H. Wu, J. Luo, H. Yu, A. Rattner, A. Mo, Y. Wang, P.M. Smallwood, B. Erlanger, S.J. Wheelan, J. Nathans, Cellular resolution maps of X chromosome inactivation: implications for neural development, function, and disease, Neuron 81 (2014) 103–119, https://doi.org/10.1016/j.neuron.2013.10.051.

[55] J. Sikora, J. Leddy, M. Gulinello, S.U. Walkley, X-linked Christianson syndrome: heterozygous female Slc9a6 knockout mice develop mosaic neuropathological changes and related behavioral abnormalities, DMM Dis Model Mech 9 (2016) 13–23, https://doi.org/10.1242/dmm.022780.

[56] S. Hayashi, Y. Inoue, S. Hattori, M. Kaneko, G. Shioi, T. Miyakawa, M. Takeichi, Loss of X-linked Protocadherin-19 differentially affects the behavior of heterozygous female and hemizygous male mice, Sci. Rep. 7 (2017) 1–15, https://doi.org/10.1038/s41598-017-06374-x.

[57] T. Ishikawa, S. Miyata, Y. Koyama, K. Yoshikawa, T. Hattori, N. Kumamoto, K. Shingaki, T. Katayama, M. Tohyama, Transient expression of Xpn, an XLMR protein related to neurite extension, during brain development and participation in neurite outgrowth, Neuroscience 214 (2012) 181–191, https://doi.org/10.1016/j.neuroscience.2012.04.030.

[58] S. Domínguez, C.C. Rey, L. Therreau, A. Fanton, D. Massotte, L. Verret, R.A. Piskorowski, V. Chevaleyre, Maturation of PNN and ErbB4 signaling in area CA2 during adolescence underlies the emergence of PV interneuron plasticity and social memory, Cell Rep. 29 (5) (2019) 1099–1112.e4, https://doi.org/10.1016/j.celrep.2019.09.044.

[59] J.Y. Min, S. Park, J. Cho, et al., The anterior insular cortex processes social recognition memory, Sci. Rep. 13 (2023) 10853, https://doi.org/10.1038/s41598-023-38044-6.

[60] A.V. Kalueff, A.M. Stewart, C. Song, K.C. Berridge, A.M. Graybiel, J.C. Fentress, Neurobiology of rodent self-grooming and its value for translational neuroscience, Nat. Rev. Neurosci. 17 (1) (2016) 45–59, https://doi.org/10.1038/nrn.2015.8.

[61] A.M. Barth, A. Domonkos, A. Fernandez-Ruiz, T.F. Freund, V. Varga, Hippocampal network dynamics during rearing episodes, Cell Rep. 23 (6) (2018) 1706–1715, https://doi.org/10.1016/j.celrep.2018.04.021.

[62] B.B.A. De Vries, A.M. Wiegers, A.P.T. Smits, S. Mohkamsing, H.J. Duivenvoorden, J.P. Fryns, L.M.G. Curfs, D.J.J. Halley, B.A. Oostra, A.M.W. Van Den Ouweland, M.F. Niermeijer, Mental status of females with an FMR1 gene full mutation, Am. J. Hum. Genet. 58 (1996) 1025–1032.

[63] D. Heine-Suñer, L. Torres-Juan, M. Morlà, X. Busquets, F. Barceló, G. Picó, L. Bonilla, N. Govea, M. Bernués, J. Rosell, Fragile-X syndrome and skewed X-chromosome inactivation within a family: a female member with complete inactivation of the functional X chromosome, Am J Med Genet Part A 122A (2003) 108–114, https://doi.org/10.1002/ajmg.a.20160.

[64] J.I. Young, H.Y. Zoghbi, X-chromosome inactivation patterns are unbalanced and affect the phenotypic outcome in a mouse model of Rett syndrome, Am. J. Hum. Genet. 74 (2004) 511–520, https://doi.org/10.1086/382228.

[65] M. Taherian, H. Maghsoudi, K. Bidaki, R. Taherian, The relationship between skewed X-chromosome inactivation and neurological disorders development, Int Clin Neurosci J (2016), https://doi.org/10.22037/icnj.v3i2.13542.

[66] J. Gribnau, T.S. Barakat, X-chromosome inactivation and its implications for human disease, bioRxiv (2017) 76–95, https://doi.org/10.1101/076950.

[67] B.R. Migeon, X-linked diseases: susceptible females, Genet. Med. 22 (2020) 1156–1174, https://doi.org/10.1038/s41436-020-0779-4.

[68] M.C. Ribeiro, J.L. MacDonald, Sex differences in Mecp2-mutant Rett syndrome model mice and the impact of cellular mosaicism in phenotype development, Brain Res. 1729 (2020) 146644, https://doi.org/10.1016/j.brainres.2019.146644.

[69] X. Zhang, Y. Li, L. Ma, G. Zhang, M. Liu, C. Wang, Y. Zheng, R. Li, A new sex-specific underlying mechanism for female schizophrenia: accelerated skewed X chromosome inactivation, Biol. Sex Differ. 11 (2020) 1–11, https://doi.org/10.1186/s13293-020-00315-6.

[70] N. Khatri, et al., The autism protein Ube3A/e6ap remodels neuronal dendritic arborization via caspase-dependent microtubule destabilization, J. Neurosci. 38 (2) (2018) 363–378, https://doi.org/10.1523/JNEUROSCI.1511-17.2017.

[71] H. Kim, P.A. Kunz, R. Mooney, B.D. Philpot, S.L. Smith, Maternal loss of Ube3a impairs experience-driven dendritic spine maintenance in the developing visual cortex, J. Neurosci. 36 (17) (2016) 4888–4894, https://doi.org/10.1523/JNEUROSCI.4204-15.2016.

[72] M. Jiang, R.T. Ash, S.A. Baker, B. Suter, A. Ferguson, J. Park, J. Rudy, S.P. Torsky, H.T. Chao, H.Y. Zoghbi, S.M. Smirnakis, Dendritic arborization and spine dynamics are abnormal in the mouse model of MECP2 duplication syndrome, J. Neurosci. 33 (50) (2013) 19518–19533, https://doi.org/10.1523/JNEUROSCI.1745-13.2013.

[73] E.A. Nimchinsky, A.M. Oberlander, K. Svoboda, Abnormal development of dendritic spines in FMR1 knock-out mice, J. Neurosci. 21 (14) (2001) 5139–5146, https://doi.org/10.1523/JNEUROSCI.21-14-05139.2001.

[74] W.G. Johnson, Metabolic interference and the + - heterozygote. A hypothetical form of simple inheritance which is neither dominant nor recessive, Am. J. Hum. Genet. 32 (1980) 374–386.

[75] M. Aarabi, E. Kessler, S. Madan-Khetarpal, U. Surti, D. Bellissimo, A. Rajkovic, S.A. Yatsenko, Autism spectrum disorder in females with ARHGEF9 alterations and a random pattern of X chromosome inactivation, Eur. J. Med. Genet. 62 (2019) 239–242, https://doi.org/10.1016/j.ejmg.2018.07.021.

[76] L.M. Dibbens, et al., X-linked protocadherin 19 mutations cause female-limited epilepsy and cognitive impairment, Nat. Genet. 40 (2008) 776–781, https://doi.org/10.1038/ng.149.

[77] S.R.F. Twigg, et al., Cellular interference in craniofrontonasal syndrome: males mosaic for mutations in the x-linked EFNB1 gene are more severely affected than true hemizygotes, Hum. Mol. Genet. 22 (2013) 1654–1662, https://doi.org/10.1093/hmg/ddt015.

[78] I. Wieland, S. Jakubiczka, P. Muschke, M. Cohen, H. Thiele, K.L. Gerlach, R.H. Adams, P. Wieacker, Mutations of the ephrin-B1 gene cause craniofrontonasal syndrome, Am. J. Hum. Genet. 74 (2004) 1209–1215, https://doi.org/10.1086/421532.

[79] C. Depienne, et al., Sporadic infantile epileptic encephalopathy caused by mutations in PCDH19 resembles dravet syndrome but mainly affects females, PLoS Genet. 5 (2009) 1000381, https://doi.org/10.1371/journal.pgen.1000381.

[80] L. Boccuto, M. Lauri, S.M. Sarasua, C.D. Skinner, D. Buccella, A. Dwivedi, D. Orteschi, J.S. Collins, M. Zollino, P. Visconti, B. Dupont, D. Tiziano, R.J. Schroer, G. Neri, R.E. Stevenson, F. Gurrieri, C.E. Schwartz, Prevalence of SHANK3 variants in patients with different subtypes of autism spectrum disorders, Eur. J. Hum. Genet. 21 (2013) 310–316, https://doi.org/10.1038/ejhg.2012.175.

[81] E. Dere, L. Dahm, D. Lu, K. Hammerschmidt, A. Ju, M. Tantra, A. Kastner, K. Chowdhury, H. Ehrenreich, Heterozygous Ambra 1 deficiency in mice: a genetic trait with autism-like behavior restricted to the female gender, Front. Behav. Neurosci. 8 (2014) 181, https://doi.org/10.3389/fnbeh.2014.00181.

[82] A.L. Gompers, et al., Germline Chd8 haploinsufficiency alters brain development in mouse, Nat. Neurosci. 20 (2017) 1062–1073, https://doi.org/10.1038/nn.4592.

[83] V. Courchet, A.J. Roberts, P Del Carmine, T.L. Lewis, F. Polleux, J. Courchet, Haploinsufficiency of autism candidate gene NUAK1 impairs cortical development and behavior, bioRxiv (2018) 262725, https://doi.org/10.1038/s41467-018-06584-5.

[84] R.M. Busch, S. Srivastava, O. Hogue, T.W. Frazier, P. Klaas, A. Hardan, J.A. Martinez-Agosto, M. Sahin, C. Eng, S.K. Warfield, B. Scherrer, K. Dies, R. Filip-Dhima, A. Gulsrud, E. Hanson, J.M. Phillips, Neurobehavioral phenotype of autism spectrum disorder associated with germline heterozygous mutations in PTEN, Transl. Psychiatry 9 (2019) 1–9, https://doi.org/10.1038/s41398-019-0588-1.

[85] E.J. Marco, D.H. Skuse, Autism-lessons from the X chromosome, Soc Cogn Affect Neurosci 1 (2006) 183–193, https://doi.org/10.1093/scan/nsl028.

[86] D.E. Godler, Y. Inaba, C.E. Schwartz, Q.M. Bui, E.Z. Shi, X. Li, A.S. Herlihy, C. Skinner, R.J. Hagerman, D. Francis, D.J. Amor, S.A. Metcalfe, J.L. Hopper, H. R. Slater, Detection of skewed X-chromosome inactivation in Fragile X syndrome and X chromosome aneuploidy using quantitative melt analysis, Expert Rev Mol Med 17 (2015), https://doi.org/10.1017/erm.2015.11.

[87] U. Moog, et al., Phenotypic spectrum associated with CASK loss-of-function mutations, J. Med. Genet. 48 (2011) 741–751, https://doi.org/10.1136/jmedgenet-2011-100218.

[88] P.A. Patel, C. Liang, A. Arora, S. Vijayan, S. Ahuja, P.K. Wagley, R. Settlage, L.E.W. LaConte, H.P. Goodkin, I. Lazar, S. Srivastava, K. Mukherjee, Haploinsufficiency of X-linked intellectual disability gene CASK induces post-transcriptional changes in synaptic and cellular metabolic pathways, Exp. Neurol. 329 (2020) 113319, https://doi.org/10.1016/j.expneurol.2020.113319.

[89] D.T. Pederick, K.L. Richards, S.G. Piltz, R. Kumar, S. Mincheva-Tasheva, S.A. Mandelstam, R.C. Dale, I.E. Scheffer, J. Gecz, S. Petrou, J.N. Hughes, P.Q. Thomas, Abnormal cell sorting underlies the unique X-linked inheritance of PCDH19 epilepsy, Neuron 97 (2018) 59–66.e5, https://doi.org/10.1016/j.neuron.2017.12.005.

[90] V.T. Dang, K.S. Kassahn, A.E. Marcos, M.A. Ragan, Identification of human haploinsufficient genes and their genomic proximity to segmental duplications, Eur. J. Hum. Genet. 16 (2008) 1350–1357, https://doi.org/10.1038/ejhg.2008.111.

[91] N. Huang, I. Lee, E.M. Marcotte, M.E. Hurles, Characterising and predicting haploinsufficiency in the human genome schierup MH, PLoS Genet. 6 (2010) e1001154, https://doi.org/10.1371/journal.pgen.1001154.

[92] H.A. Shihab, M.F. Rogers, C. Campbell, T.R. Gaunt, HIPred: an integrative approach to predicting haploinsufficient genes, Bioinformatics 33 (2017) btx028, https://doi.org/10.1093/bioinformatics/btx028.

[93] J. Steinberg, F. Honti, S. Meader, C. Webber, Haploinsufficiency predictions without study bias, Nucleic Acids Res. 43 (2015) 101, https://doi.org/10.1093/nar/gkv474.

[94] Y. Yang, S. Li, Y. Wang, Z. Ma, K.-C. Wong, X. Li, Identification of haploinsufficient genes from epigenomic data using deep forest, Brief Bioinform (2021), https://doi.org/10.1093/bib/bbaa393.

[95] P. Przanowski, et al., Pharmacological reactivation of inactive X-linked Mecp2 in cerebral cortical neurons of living mice, Proc Natl Acad Sci U S A 115 (2018) 7991–7996, https://doi.org/10.1073/pnas.1803792115.